Politecnico di Milano

SCHOOL OF INDUSTRIAL AND INFORMATION ENGINEERING

Master of Science – Electrical Engineering

DESIGN of WIRELESS POWER TRANSFER COIL useful in HIGH POWER CHARGING of ELECTRIC VEHICLE

Supervisor

Prof. Alberto Dolara

Candidate

Saumitra Pal Choudhori – 882502

Academic Year 2017 – 2019

I don't care that they stole my idea . . .
I care that they don't have any of their own

-Nicola Tesla

Abstract

Inductive power transfer (IPT) technology is becoming more and more attractive for electric vehicle charging due to its safe, flexible and convenient features such as no need to plug the cable, just park and forget as the transfer of energy does not need any cables it can start once aligned with the receiver. Although attractive, IPT suffers from the large leakage inductance, especially when there is misalignment between the pads. The misalignment reduces the coefficient of coupling and hence reduces the overall efficiency of the system.

The aim of this thesis is to design and simulate the Bipolar Pad in order to have a higher power available in the receiver side which can be utilised for fast charging of the battery and also have a system which has higher tolerance for misalignment. Hence we propose here the use of double-sided LCC compensation network with which the resonant frequency is independent of load condition and coupling coefficient, thus system can work in wider range of frequency and have better efficiency.

The proposed model here is Bipolar Pad with modular design as each of the transmitter coils are independently driven by the source so if there is no sufficient alignment with the receiver coil then each of the coil can be turned off independently. Even the receiver side coils with the battery system is kept independent to each other so that in case of misalignment there is no circulating current between the two coils. Even BPP being in receiver side can be interoperable to work with other pad structure like from Circular pad transmitter.

The model is simulated and verified using the Finite Element Analysis of Ansys Maxwell to find the proper coefficient of coupling, core loss, magnetic saturation and using the power electronics model in Ansys Simplorer to find the amount of power which can be transferred using this model.

This thesis is presently limited to only the transfer of power between the coils and the converters involved for AC/AC and AC/DC conversion is not taken into consideration. An ideal voltage source with a frequency of 85KHz is considered and the load is considered as a equivalent resistor for the limitation of this thesis.

Abstract

Le tecnologie per il trasferimento di potenza elettrica per via induttiva (IPT) applicate alla ricarica dei veicoli elettrici stanno diventando sempre più di interesse grazie alle loro caratteristiche di sicurezza, flessibilità e convenienza, come ad esempio la mancanza del cavo di collegamento: basta parcheggiare il veicolo in modo che trasmettitore e ricevitore siano allineati perché il trasferimento di energia possa avere inizio. Anche se adatta alla ricarica dei veicoli, la tecnologia IPT presenta alcune limitazioni principalmente dovute all'elevata induttanza di dispersione, soprattutto quando i pad sono disallineati. Il disallineamento riduce il coefficiente di accoppiamento e quindi riduce l'efficienza complessiva del sistema. Lo scopo di questa tesi è quello di progettare e simulare un pad di tipo bipolare in modo da massimizzare la potenza disponibile al ricevitore, che è utilizzato per la ricarica rapida della batteria di un veicolo elettrico, e garantire anche una maggiore tolleranza al disallineamento dell'intero sistema. Viene analizzato l'utilizzo di una rete di compensazione LCC sia sul lato di trasmissione che sul lato di recezione: tale schema di compensazione permette di rendere indipendente la frequenza di risonanza dalla condizione di carico e dal coefficiente di accoppiamento. Ciò permette al sistema IPT di funzionare in una più ampia gamma di frequenze ed avere una migliore efficienza. Il modello proposto in questo lavoro è un pad bipolare dal design modulare, in quanto ciascuna delle bobine del trasmettitore è alimentata da una sorgente indipendente; nel caso in cui vi sia un disallineamento elevato, ogni singolo avvolgimento può essere disattivato in modo indipendente. Anche le bobine del ricevitore sono indipendenti l'una dall'altra, in modo che in caso di disallineamento non vi sia corrente di circolazione tra le due bobine. Anche il pad bipolare lato ricevitore può essere interoperabile, per lavorare con pad di altra forma e struttura come ad esempio un trasmettitore formato da un pad circolare. Il modello dei pad è simulato e verificato utilizzando l'analisi agli Elementi Finiti di Ansys Maxwell al fine di calcolare il corretto coefficiente di accoppiamento, le perdite nel nucleo e gli effetti della saturazione magnetica. Il modello dell'intero sistema di trasmissione dell'energia è implementato in Ansys Simplorer, da esso si ricava la quantità di potenza che può essere trasferita utilizzando questo sistema. Questa tesi è attualmente limitata solo all'analisi del trasferimento di potenza tra i pad, il modello

dettagliato dei convertitori AC/DC e DC/AC utilizzati per la conversione dell'energia non sono presi in considerazione. L'alimentazione AC in alta frequenza è rappresentata da un generatore di tensione ideale con una frequenza di 85 kHz, mentre il carico è rappresentato da resistenza equivalente.

Contents

List of Figures

x

List of Tables

Acronym

3D	Three Dimensional
A	Ampere
AC	Alternating Current
BPP	Bipolar Polarised Pad
CP	Circular non polarised Pad
CC	Constant Current
CV	Constant Voltage
DC	Direct Current
DDP	Double-D polarised Pad
DDQP	Double-D Quadrature polarised Pad
EM	Electro Magnetic
IPT	Inductive Power Transfer
k	coefficient of coupling
KHz	Kilo Hertz
LCC	Inductor-Capacitor-Capacitor Compensation
Q	Quality factor
Rx	Receiver side
RMS	Root Mean Square
TPP	Tripolar Polarised Pad
Tx	Transmitter side
WPT	Wireless Power Transfer
WWS	World Wireless System
ZPA	Zero Phase Angle

Introduction

Wireless Power Transfer is a way of transferring electrical energy from one source to another over an air gap without the direct physical contact [1]. This was first experimented by Nicola Tesla in late 19th century [2] with the use of microwaves. In Colorado Springs, Colorado USA, in 1900, he built a tree-shaped tower, 200 feet high, with a copper ball at the top. With a frequency of 150 kHz, and 300 kW input power, it was able to spread discharge up to 50 km from the source.

Subsequently Tesla built the Wardenclyffe tower as seen in Fig. 1, on Long Island, a large structure in high voltage, high 154 feet, with a copper electrode of 20.7 m in diameter in toroid form. The latter shows the futuristic vision of Tesla, according to which one day we would have a "WWS (World Wireless System)", able to electrify the entire globe, without the need for physical connections.[3]
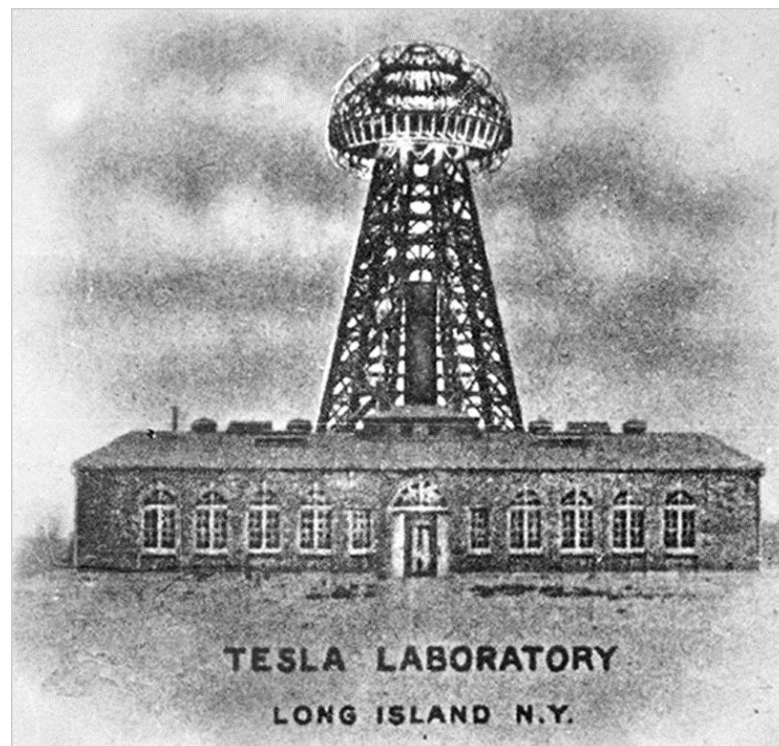
Figure 1: Wardenclyffe Tower

WPT today can be classified into radiative coupling, non-radiative capacitive coupling and non-radiative magnetic coupling.

Radiative WPT coupling is not very convenient to transfer very large power like microwave or laser, uses electromagnetic radiation for far-field transmission. However, due to its omnidirectional behaviour the efficiency is quite low, and thus its much beneficial to transmit information than power [4][5].

Non-radiative capacitive coupling WPT uses an electric field from a capacitive coupling for near-field transmission. This technology is not chosen widely as high voltages are required to transfer any significant amount of power and the intensity of the electric field will definitely harm the human body [4].

Non-radiative magnetic coupling is a near-field transmission technology which uses a magnetic field rather than electric field to transfer power over an air gap [4]. Transformers, electrical machines, and wireless charges are electrical devices that make use of non-radiative magnetic coupling WPT, which is also often referred to as contactless power transfer (CPT) or inductive power transfer (IPT). One of the most common magnetic coupling WPT is the resonant IPT. The resonant IPT is similar to using transformers but the coils are connected to capacitors in different topologies in order to create resonance (typically between 20 kHz and a few MHz).

The most latest starting point of wireless electricity was when WiTricity research group, in collaboration with the prestigious US university MIT, introduced a true wireless electrical transformer in 2007, who was able to power a 60W bulb to 2m away as shown in figure 2.

Figure 2: Research Lab at MIT where the experiment was conducted in 2007 by researchers WiTricity
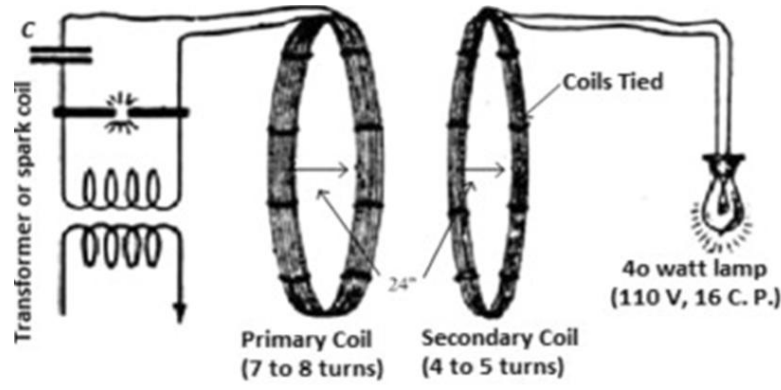
Figure 3: Setup scheme of the circuit experiment
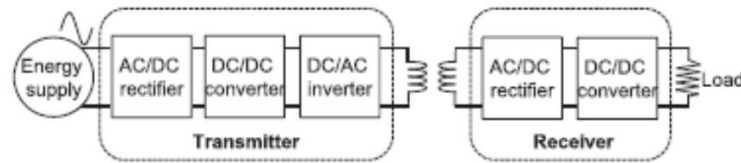
Figure 4: Typical WPT system [6]

As seen in the Fig. 4 we have the mains AC supply at 50/60 Hz and this frequency is not suitable for inductive power transfer and hence we have convert the AC to DC after which we have DC/DC converter to regulate the DC voltage which is then fed to DC/AC inverter for the AC signal at desired voltage and frequency which is around 20-100 KHz, and this is fed to the transmitter coil. The receiver coil which is at a certain distance from the transmitter coil gets induced a voltage due to the variation of magnetic field flux from the transmitter coil, thus working similar to an air core transformer.

The inductive coupling uses the physical phenomenon of induction produced by the varying flux as the means of transferring energy between the coils. For an effective transfer of energy, the distance between the 2 coils is usually less than one wavelength of the frequency used for the inductive coupling, usually its in the range of 20-100 kHz .

The orientation of secondary coil w.r.t the primary coil has a significant impact on the efficiency of energy transmission. As in figure 5 we can find in one case that the flux linkage is maximum in the secondary coil and hence this will involve in higher efficiency of energy transfer. While in the other case when the secondary coil is aligned with the magnetic field in such a way that the flux linkage is minimal, hence the coupling between
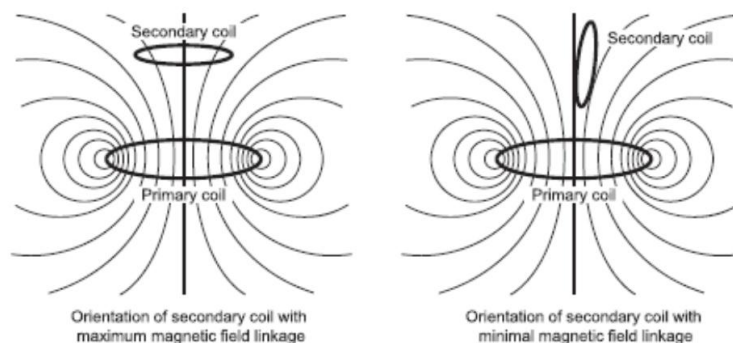
Figure 5: Orientation of the coils showing maximum and minimum magnetic connection

the coil will be very low and thus least energy transfer efficiency.

Thus, the advantages of wireless energy transfer based on inductive coupling ca be listed as below:

1. It is easy to implement
2. It can work in flexible manner
3. It has higher efficiency for a shorter distance transfer of energy
4. It can have lower cost in comparison to other coupling type

Hence for our thesis we work on the non-radiative inductive coupling system for wireless power transfer.

Thesis Outline

This thesis with the objective of "higher power transfer and better misalignment tolerance" is organised into the following chapters :

Chapter 1 : Literature Review

This chapter discuss about the State of Art of Wireless Power Transfer that has been researched and worked upon until now with each of different coil structures having its own advantage and disadvantage and thereby the reason to choose Bipolar pad for designing.

Chapter 2 : Designing in Ansys Maxwell 3D

This chapter describes about how the Bipolar pad is designed using the tools in Ansys Maxwell to represent the lumped model of the real world model.

Chapter 3 : Magnetostatic Solution Setup

This chapter describes about the setup of Ansys Maxwell in magnetostatic solution type which is needed initially to find the mutual inductance between the two coils of transmitter and receiver side and after this we setup this into eddy current for our further simulation.

Chapter 4 : Eddy Current Solution Setup

This chapter describes about how the setup from chapter 3 is imported here and then is setup for eddy current solution type which is simulated further to be used as a dynamic equivalent circuit in Ansys Simplorer.

Chapter 5 : Results and discussion of Maxwell 3D

This chapter includes all the results obtained in Ansys Maxwell 3D which we analyse towards the objective of our thesis.

Chapter 6 : Ansys Simplorer Setup

This chapter describes about the set up of power electronic circuit to be used for the WPT and we can analyse the power transmitted and received, even the voltage and current can be analysed, thus verifying our model.

Chapter 7 : Results and discussion of Ansys Simplorer

This chapter includes all the results obtained by the analysis in Ansys Simplorer

Conclusion

This section deals with the conclusion of the thesis and proposes ideas of the future work within this Master thesis.

Chapter 1

Literature review

As we have to deal with near field power transfer and from the introduction chapter we have decided to choose non-radiative magnetic coupling WPT system, now Non-radiative magnetic coupling WPT can be done using various coupler configurations [7][8]. They are listed as follows:

1. Circular non polarized Pad (CP)
2. Flux Pipe / Solenoid
3. Double-D polarised Pad (DDP)
4. Double-D Quadrature polarised Pad (DDQP)
5. Bipolar polarized Pad (BPP)
6. Tripolar polarised Pad (TPP)

The coupler consists of transmitter and receiver being the most important part of WPT. The desired characteristics for coupling pads are high coefficient of coupling 'k', quality factor 'Q', and high misalignment tolerance [8].

1.1   Circular non polarized Pad (CP)

As mentioned in [8][9] these are the most commonly used coil structure since early 2000's and it became popular because of the single-sided magnetic field that enters and leave the coil only from the front side.

The single sided nature of flux pattern helps in reducing leakage flux [8]. As shown in figure 1.1, ferrite bars are presented to the back of the coil pad to facilitate a low

Fe_w Ferrite width
Fe_L Ferrite length
δ_Al Extended Rad.
C_d Coil Dia.
P_d Pad Diameter
C_w Coil width
25 turn coil (Ø4mm
Litz). 10mm thick ring
I_1 = 23A at 20kHz
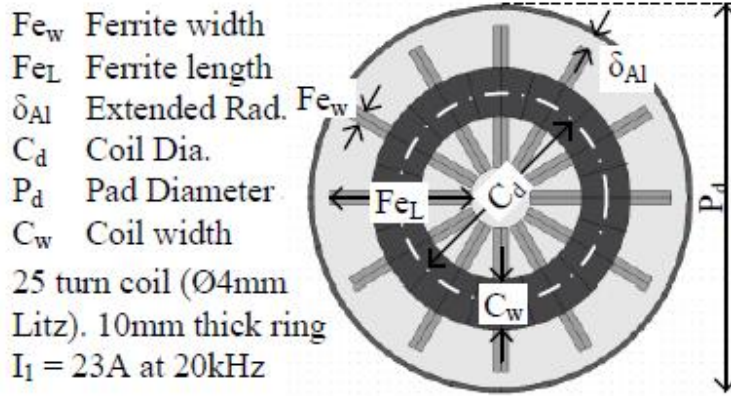
Figure 1.1: Typical layout of a circular pad [9]
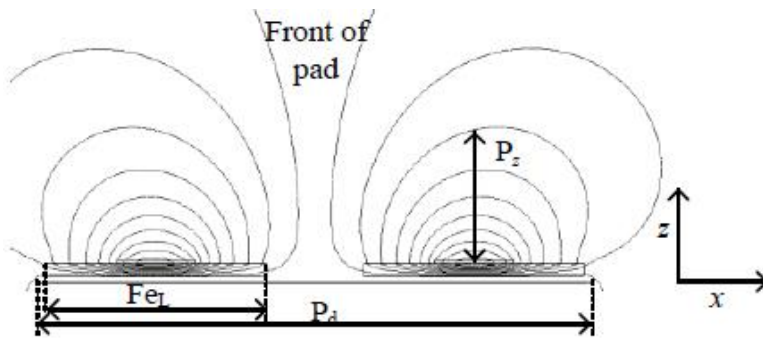
Figure 1.2: Typical filed generated in circular pad [9]

reluctant flux path and also reduce the flux leakage [7]. An aluminium plate is placed on the back of the whole coil in order to hold up the flux distribution. This topology gives the advantage that the structure is easy to build with the symmetric flux distribution around the centre but the flux height is proportional to half of the ferrite length is a quarter of pad diameter (Pd/4) as mentioned in [9].

But this configuration has lower tolerance to misalignment which can occur very easily while parking the vehicle and hence there were other configurations that got developed to improve the tolerance to misalignment and also improve the flux height.
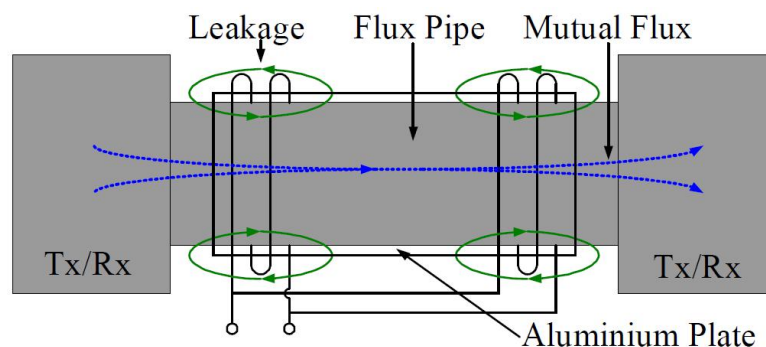
Figure 1.3: Typical layout of solenoid pad [10]

1.2   Flux Pipe / Solenoid

The flux pipe consists of two coils positioned at ends of the midsection of a pad as shown in Fig. 1.3. The Tx and Rx are the flux transmitting and receiving surfaces, both track and pickup pads are identical. The coils are electrically connected in parallel to lower the impedance and are connected magnetically in series since flux from one coil passes through to the other. The mutual flux between coils links with the pickup pads to couple power [10]. They were developed and used in monorail automated guided vehicle in 90's [9].

Here the fundamental flux path is half of the length of the receiver pad and hence it is better than circular pad . The coefficient of coupling is also similar to the circular pad but the drawback of this design is that the quality factor and the efficiency of the system reduces when aluminium shielding is used [8].

1.3   Double-D polarised Pad (DDP)

This is a polarised single-sided flux coupler that combines the advantage of both flux pipe as well as circular pad design [8]. The middle of the DD coil is similar to flux pipe as the coils are connected in series magnetically [8]. Here the coils are placed on top of ferrite and the aluminium shield is placed under the ferrite thus no loss in quality factor. Thus this DDP design has higher coefficient of coupling, lower losses in aluminium shielding and lower leakage flux also flux height is proportional to half the length of the pad [8]. Thus it is a great improvement over the circular pad design.

As a receiver pad the DD coil can only couple horizontal flux component when centred
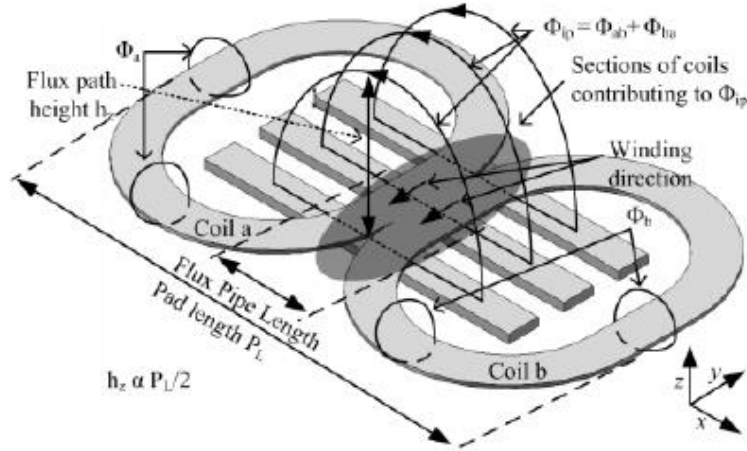
Figure 1.4: Simplified model of DD pad [9]

with a transmitter pad, whereas the circular pads can only couple vertical flux component when aligned centrally [9]; also this topology has poor interoperability characteristic when the receiver pad is centrally aligned with the transmitter pad, same goes for the CP topology [7], this led to the development of DDQP pads which can overcome this interoperability issues.

1.4 Double-D Quadrature polarised Pad (DDQP)

The DDQP topology was designed to generate the both parallel and perpendicular magnetic field [7]. In this topology an additional coil is placed on DDP topology, which is shown in figure 1.5 . As the DDQP topology can generate both the polarized and non-polarized field by regulating the coil current, the flexibility of the system is high than any other topologies, hence higher tolerance to misalignment. But the disadvantage is the increased number of coils, which leads to the increased cost of the topology [7]. This increase in coils is about three times with respect to circular pad [8].

1.5 Bipolar polarised Pad (BPP)

In this topology coil A and coil B are overlapped in such a manner so that they are mutually decoupled as shown here. This topology overcomes the added coil structure of
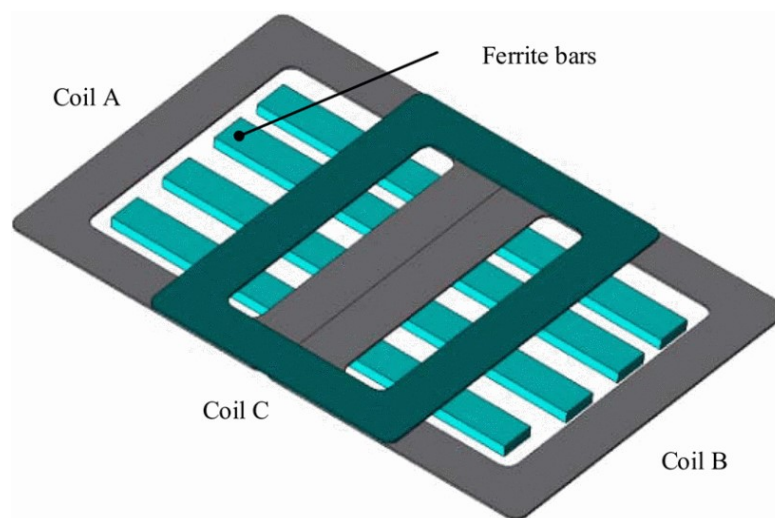
Figure 1.5: Typical model of DDQ polarised pad [7]
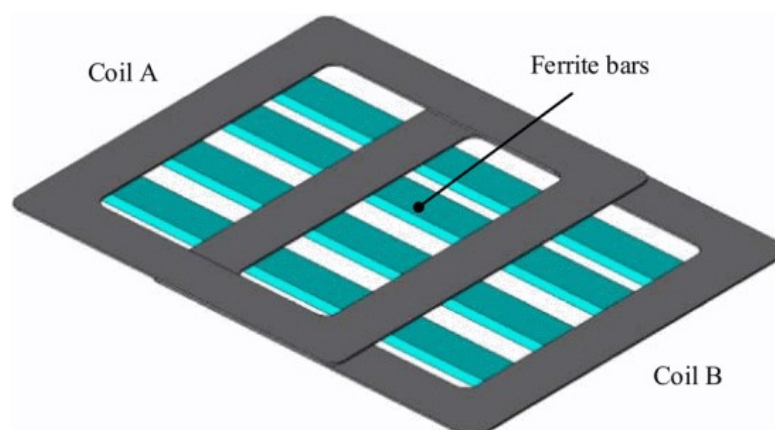
Figure 1.6: Typical model of Bipolar polarised pad [7]

DDQP topology hence the copper used here is around 25% to 30% lesser [8] than DDQP topology making this lesser expensive compared to DDQP. And this topology has similar performance to DDQP with regard to misalignment tolerance and higher coefficient of coupling [8]. As per different operation of current direction, BPP can work as CP, single coil or DD mode and thus most suitable for multi-mode secondary pad design [7].
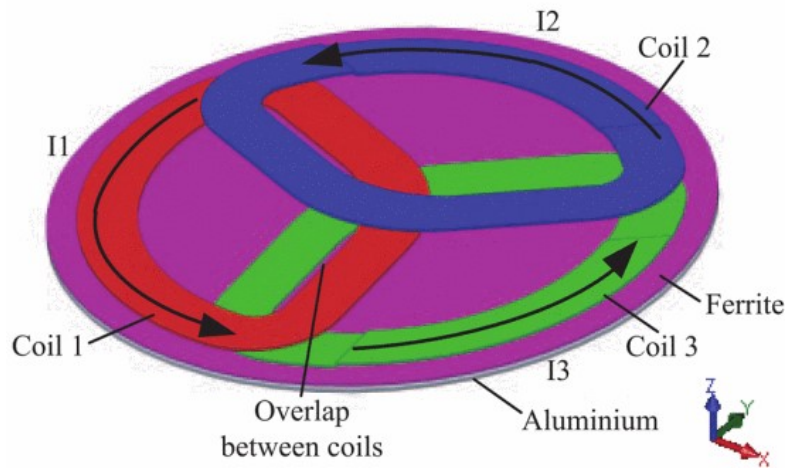
Figure 1.7: A typical a Tripolar pad with arrows showing the flow of current in phase [11]

1.6   Tripolar polarised Pad (TPP)

Tripolar pad (TPP) is a three-coil coupler arranged in such a way that they are mutually decoupled as shown in Fig. 7 [11]. This topology allows high tolerance to rotational misalignment of a non-polarized pad [11].

The three mutually decoupled coils are driven independently to achieve highest coupling factor which can be seen in block diagram. As in [11] in this topology allows an increase in effective coefficient of coupling with bipolar and circular pad as the secondary coil. This was accomplished by controlling voltage magnitude and phase of the transmitter coil currents. The apparent power demand is reduced by 45% compared to the circular pad for an air gap of 150 mm [11]. The leakage magnetic field reported is also less. However, the need for three separate inverters to drive three mutually decoupled coils adds to its cost and increases complexity of control [11].
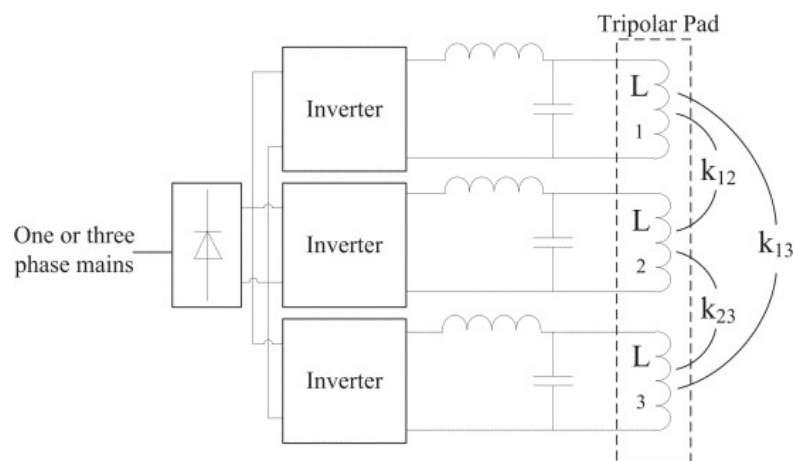
Figure 1.8: Block diagram of a Tripolar pad as a primary for an IPT system [11]

1.7 Comparison of different topologies for coil configuration

Coil Topology	Misalignment Tolerance	Coefficient of Coupling	EMF exposure	Effect of shielding on coefficient of coupling	Magnetic Flux Direction
Circular Pad	Poor	Low	High	Low	Single sided
Flux Pipe	Medium	Medium	Low	High	Double Sided
DD Pad	Poor	High	Low	High	Double Sided
DDQ Pad	High	High	Low	High	Double Sided
Bipolar Pad	Medium	High	Low	High	Double Sided
Tripolar Pad	High	High	Low	Low	Single Sided

Table 1.1: Performance comparison of different coil topology as discussed in [8]

Coil Topology	Transferable Power	Size of Pad	Weight of Pad	Material Cost of System	Transmission Distance	Charging Zone
Circular Pad	Medium	Medium	Low	Low	Low	Small
DD Pad	High	Small	Low	Medium	Medium	Medium
DDQ Pad	High	Small	Medium	High	High	Large
Bipolar Pad	High	Small	Medium	Medium	High	Large
Tripolar Pad	High	Medium	High	High	High	Large

Table 1.2: Comparison of different coil topology as discussed in [7] [11]
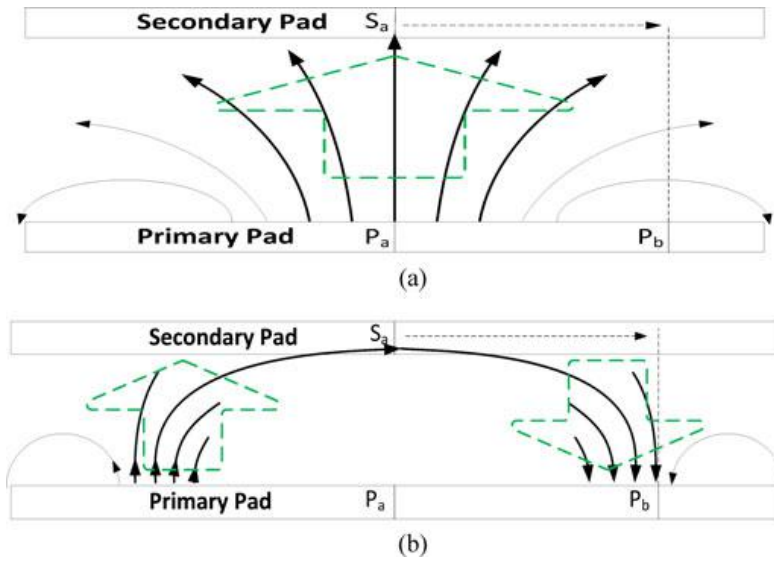
Figure 1.9: Simplified 2D view of a)perpendicular field pattern and b)parallel field pattern [12]

1.8 Coil Topology and their features

1.8.1 Circular Pad Topology

- Flux symmetric around CP centre
- Non polarised perpendicular field pattern by CP
- Commonly used in primary and secondary
- Poor interoperability characteristics
- Generate and couple perpendicular flux
- Flexible application

1.8.2 DD Pad Topology

- Single sided flux generation
- Better performance of interoperability with different topologies
- Commonly used in primary
- Ferrite bars are easy to saturate at high power rate
- No reverse flux to eliminate the unwanted rear flux

1.8.3 DDQ Pad Topology

- As a secondary the charge zone provide is three time of DD pad

- Better performance than DD with different secondary topologies
- Commonly used in secondary
- Variable excitation modes
- Versatile in central coil design to fit the air gap

1.8.4 Bipolar Pad Topology

- Mutually decoupled partially overlapped structure
- Almost same performance and identical power to DDQP
- Uses lesser copper than DDQ
- Commonly used in secondary

1.8.5 Tripolar Pad Topology

- High tolerance to rotational displacement
- All three coils mutually decoupled and overlapped, can be controlled individually
- TPP as primary maintains a high level of uncompensated power regardless of any rotational displacement

1.9 Chosen coil topology for the project

From the above section 1.8 and Table 1.1, Table 1.2 we can find out that the Bipolar Pad Topology has higher advantages compared to any other topology with respect to cost to weight of copper used vs interoperability between different topologies, misalignment tolerance and charging zone. And hence after all these comparison it was decided to choose the designing of Bipolar Pad Topology.

1.10 Compensation Topologies

To transmit power wirelessly, using a loosely coupled transformer it involves a large winding separation which has a relatively large leakage inductance, as well as proximity effect and winding resistance, even magnetising flux is significantly reduced [13]. Thus additional compensation capacitors are needed to form the resonant tanks in both primary as well as secondary side [13]. Usually the primary side inductance is compensated/-tuned to decrease the apparent power supply rating and the secondary inductance is compensated/tuned to maximize power transfer [12].

The most basic requirement of a compensation capacitor is to resonate with primary/secondary inductance to provide the reactive power required for the generation of adequate magnetic fields [14].

1.10.1 Compensation Requirements

As written in paper [13]

- Minimum VA rating and maximized power transfer capability

    Minimises apparent power / VA rating of power supply

    Cancels the secondary inductance to maximize transfer capability

- Constant-Current(CC) / Constant-Voltage(CV)

    Compensation topology can be selected as per the output requirement CC or CV

- High Efficiency

    Its mainly decided by coupling coefficient and quality factor of the windings

- Bifurcation Resistant

    To guarantee system stability by having unique zero phase angle (ZPA)

1.10.2 Basic Compensation types

a) Series-Series Compensation

In this scheme the compensation capacitance is placed in series with the winding inductance both in the primary as well as secondary side.

b) Series-Parallel Compensation

Here the primary side is connected in series to the compensation capacitance and secondary side is connected in parallel. This design is usually adopted for a constant-voltage output.

c) Parallel-Series Compensation

Here the primary side is connected in parallel to compensation capacitance and secondary side is connected in series

d) Parallel-Parallel Compensation

In this scheme the compensation capacitance is placed in parallel with the winding inductance both in the primary as well as secondary side.

These compensation types can be realised in the figure 1.10 .
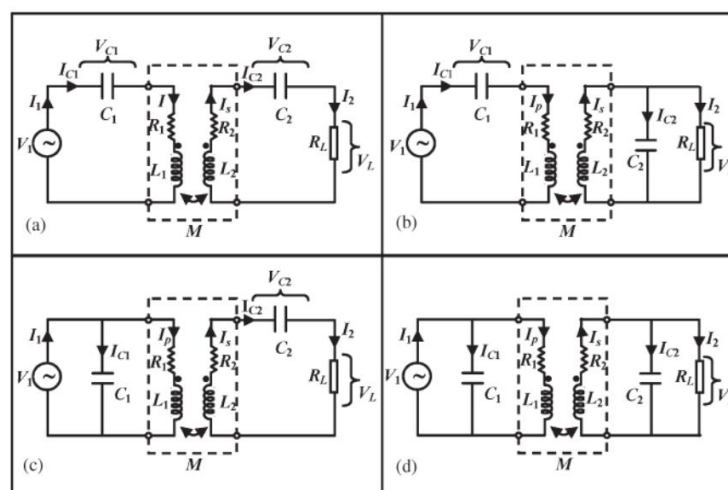
Figure 1.10: Connection of different compensation topologies

When the compensation capacitor is connected in series in the primary side it acts as a voltage generator and when connected in parallel with an inductor the capacitor becomes a current generator.

On the secondary side the capacitor is dimensioned in order with the secondary coil inductance so as to minimize the circulating apparent power.

The Capacitor C_1 can be calculated from the Table 1.3 below :

Compensation topology	Primary capacitance C_1
Series-Series	$\frac{C_2 L_2}{L_1}$
Series-Parallel	$\frac{C_2 L_2^2}{L_1 L_2 - M^2}$
Parallel-Series	$\frac{C_2 L_2}{\frac{M^4}{L_1 C_2 L_2 R_L} + L_1}$

Parallel-Parallel	$\dfrac{(L_1 L_2 - M^2) C_2 L_2^2}{\frac{M^4 C_2 R_L}{L_2} + (L_1 L_2 - M^2)^2}$

Table 1.3: Mathematical equation for different compensation [8]

	Series-Series	Series-Parallel	Parallel-Series	Parallel-Parallel
Dependence on load resistance and coefficient of coupling factor	Primary and secondary compensation capacitor are independent of load and coupling	Secondary compensation capacitor is dependent on load and coupling factor	Primary compensation capacitor is dependent on load and coupling factor	Primary and secondary compensation capacitor are dependent of load and coupling factor
Inverter device voltage rating	Lower DC link voltage is required (higher than SP)	Lower DC link voltage	Higher voltage is needed as compared to SS and SP	Higher voltage is needed as compared to SS and SP
Inverter device current rating	Primary Coil current	Primary Coil current	Active component of the primary coil current	Active component of the primary coil current

Table 1.4: Comparison of different Compensation Network [8]

1.11 LCC Compensation

This is a modified kind of compensation which is mentioned in [15], [16] and [17] and they have mentioned the benefits in this kind of compensation. The most useful one being that it can operate in the frequency independent of coupling coefficient and loading condition, also can be understood as decoupling of secondary currents and the load. Besides it has better tolerance to misalignment position, higher efficiency and lower sensitivity of changing mutual inductance between the coils [16], [15].

The figure 1.11 represents the typical LCC compensation configuration used for the WPT system.

Here it can be analysed that a tuning circuit is added to the Series-Series compensation topology in order to increase the efficiency by changing the resonant frequency to match the operating frequency. This double sided LCC topology consists of one inductor
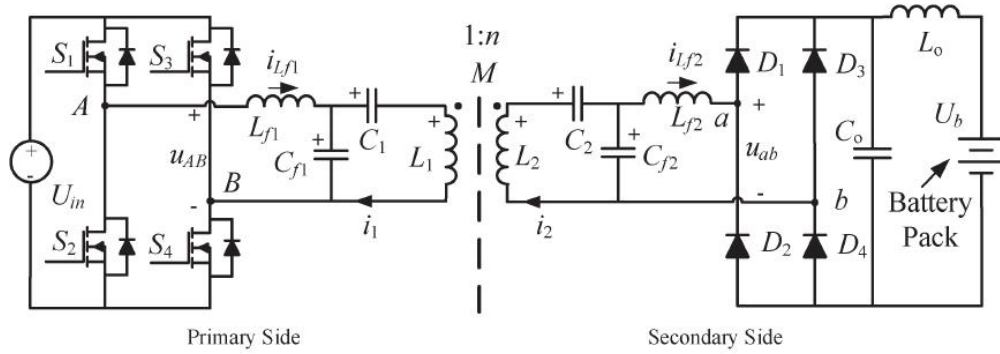
Figure 1.11: Double-sided LCC compensation topology for WPT [16]

and two capacitors at both the primary as well as secondary side, and with this method the resonant frequency of the compensated coils is independent of the coupling coefficient and the load condition.

In regard to figure 1.11 we will deal only with the compensation for now and exclude the converters and rectifiers. Here L_1 and L_2 denotes the self inductance of the transmitter and receiver coil respectively. But in our model we have 4 coils namely two each in transmitter and receiver side. Hence in our model we denote L_1, L_2 as the self inductance of transmitter side coils and L_3, L_4 of the receiver side respectively. Similarly, in the figure L_{f1}, C_{f1} and C_1 are transmitter side compensation inductance and capacitance and L_{f2}, C_{f2} and C_2 for receiver side compensation respectively. But as said before we have 4 coils in our model and hence the subscript 1,2 represents transmitter side and 3,4 as for receiver side.

The calculation of L_{f1}, C_{f1}, C_1, L_{f2}, C_{f2} & C_2 is done using the equations as follows [16]:

$$L_{f1}C_{f1} = \frac{1}{w_0^2} \tag{1.1}$$

$$L_{f2}C_{f2} = \frac{1}{w_0^2} \tag{1.2}$$

$$L_1 - L_{f1} = \frac{1}{w_0^2 C_1} \tag{1.3}$$

$$L_2 - L_{f2} = \frac{1}{w_0^2 C_2} \tag{1.4}$$

Part I

Ansys Maxwell 3D

Chapter 2

Designing in Ansys Maxwell 3D

Before we begin with the designing of the coil we can go through the steps needed for taking the consideration for the initial design.
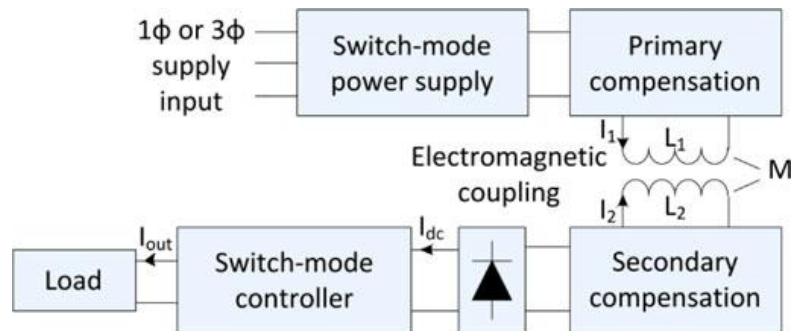

Figure 2.1: Block diagram of a typically loosely coupled IPT system [12]

To consider for the size of the coil to be used first we take an estimate measurement of a car as seen in Fig. 2.2.

2.1   Windings Size Calculation

For determining the winding size we can follow the paper [18] which can be seen in the Fig. 2.3
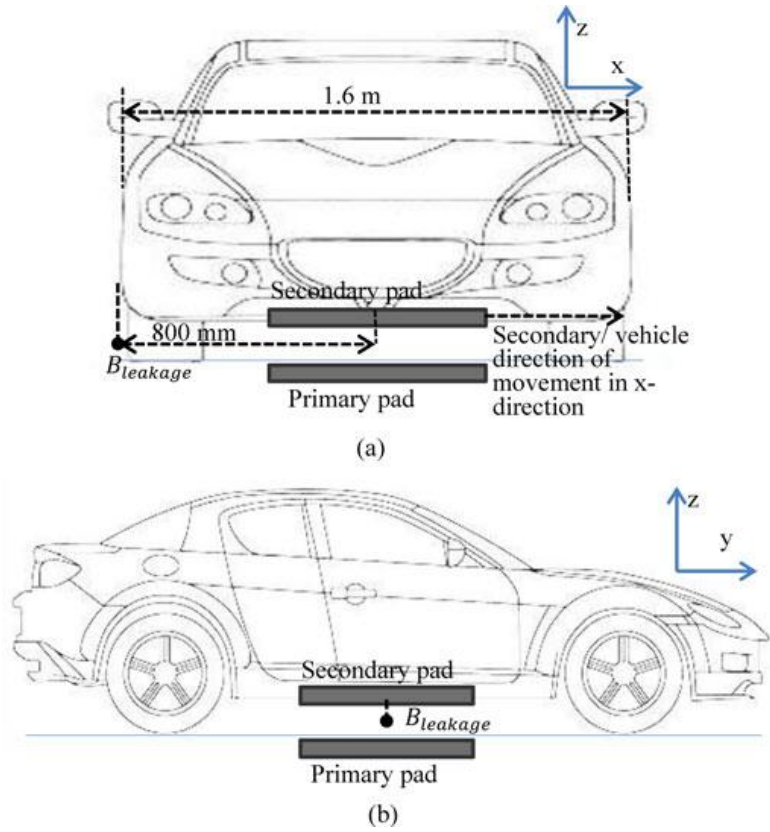
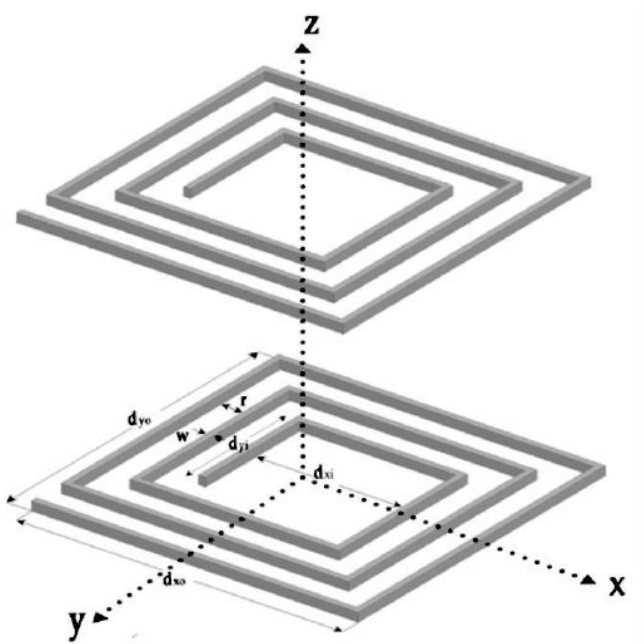Figure 2.2: Dimension of a typical vehicle for the placement of the coil [12]

Figure 2.3: Typical rectangular coil between primary and secondary winding of a WPT system [18]

The equation 2.1 gives the details of calculation of winding size to be implemented in Ansys 3D from the figure 2.3.

$$d_{xo} = d_{xi} + 2 * [N * w + (N - 1) * \gamma] \qquad (2.1)$$

d_{xo} = Outer side of the winding

d_{xi} = Inner side of the winding

N = Number of turns of the coil

w = cross-sectional width of the coil

γ = spacing between consecutive turns

For the sake of easy calculation in ANSYS we will use a lumped model which can reduce the simulation complexity.

2.2   Coil Design

As discussed in chapter 1 with the different types of coil topologies we found that BPP coil topology has better advantages over the other topologies mentioned over misalignment and inter operability between different topology for higher power transfer. Hence we designed the BPP coil using ANSYS Maxwell 3D.

The coil 1 is drawn using the function 'Draw Line', and hence a square shaped coil is drawn as shown in figure 2.4.
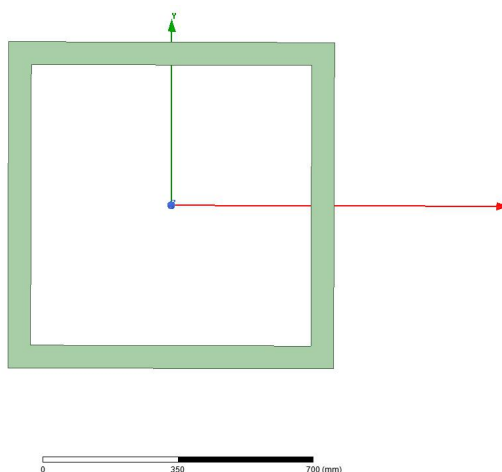

Figure 2.4: Coil 1 in Ansys Maxwell 3D

We have taken this as a lumped model considering each copper wire to be of 12mm with 5 turns of coil in total and hence the total width comes as 60mm which can be confirmed from equation 2.1.

And after this coil 1 is drawn, the next coil 2 is drawn which has to be placed mutually decoupled to coil 1. This process is described in section 2.2.1.Thus after drawing both the coils the overall transmitter coil 1 and coil 2 can be seen as in Fig. 2.5.
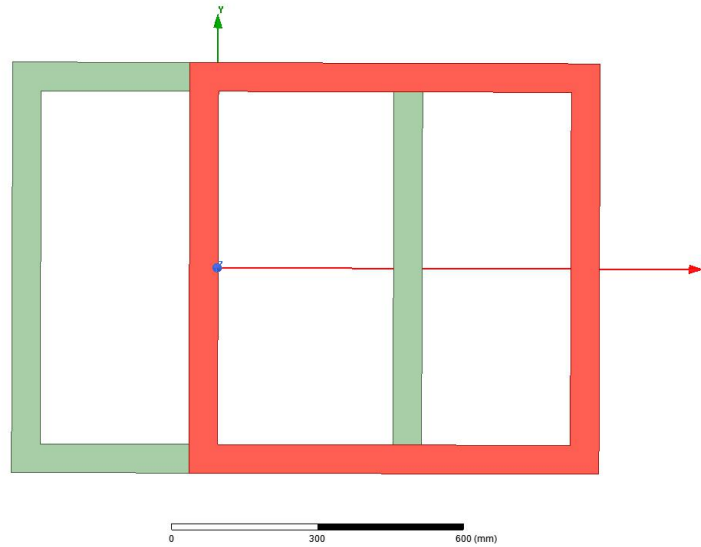

Figure 2.5: Coil 1 and Coil 2 in Ansys Maxwell 3D

Similarly coil 3 which is perpendicular to coil 1 and coil 4 which is perpendicular to coil 2 is drawn keeping a distance of 120mm (which is considered as air gap between the ground and the chassis of the car) between the upper and lower coils which acts as receiver and transmitter respectively as shown in Fig. 2.6.

The following Table 2.1 shows the properties of the coil model that was used in Ansys.

2.2.1 Mutual decoupling between the 2 coils of transmitter and receiver

From the papers [19] and [15] it has been clearly mentioned that when we have to make the overlap between the two coils in such a manner that the two coils of transmitter and receiver has the least coupling coefficient between both of them.

Thus in this model we start increasing the overlap and at the same time checking for the coupling coefficient until we find the point which is close to zero. This demonstration
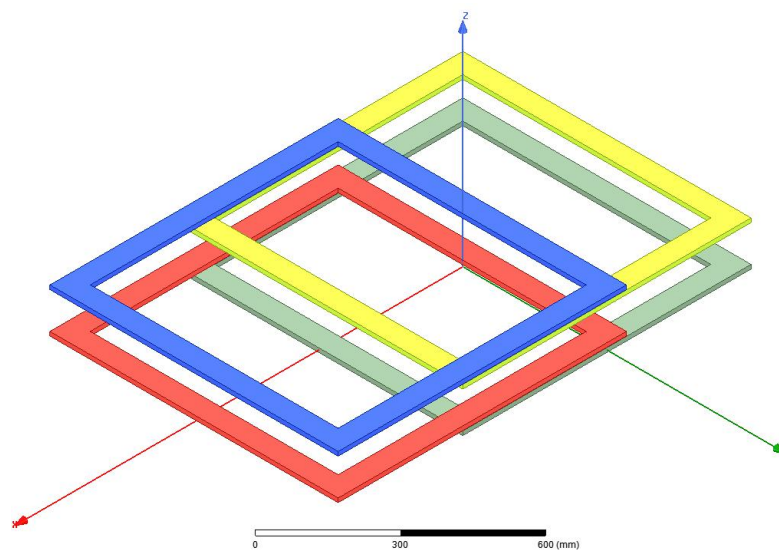
Figure 2.6: Model of the Receiver and Transmitter coils in air

Number of points	5
Number of curves	4
Width/Diameter	80mm
Height	4mm
Relative permittivity	1
Relative permeability	0.999991
Bulk Conductivity	58000000 siemens/m
Mass Density	8933 kg/m^3
Area of each coil	460800mm^2
Volume of each coil	2304000mm^3
Weight of each coil	20.581632 Kg

Table 2.1: Coil model properties in Ansys

can be seen in the figure 2.7 and we can see that at certain overlap distance the coupling coefficient is close to zero and after certain point it starts increasing again. Thus this is the overlap distance where we need to place the coils in order to have decoupling between them.
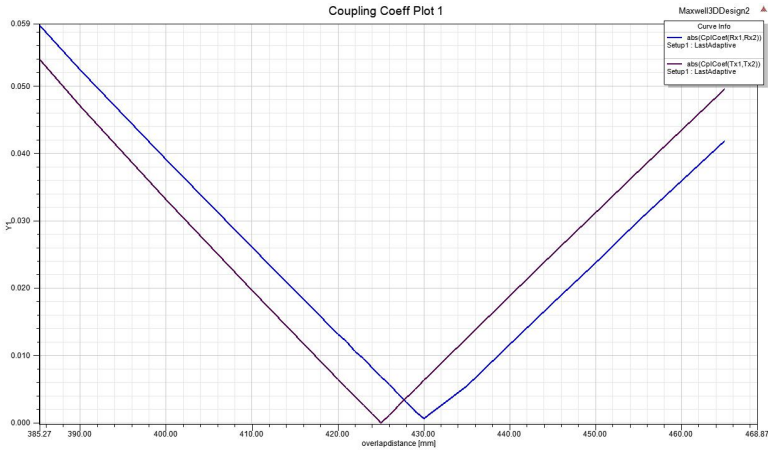
Figure 2.7: Mutual Coupling Coefficient vs Overlapping distance

2.3 Ferrite Design

The ferrite model was designed similarly using the function 'Draw Line', and was chosen seven number of ferrites for the entire coil. The bottom view of the ferrite below the coil 1 and coil 2 is as shown in figure 2.8 by the cyan coloured bars.
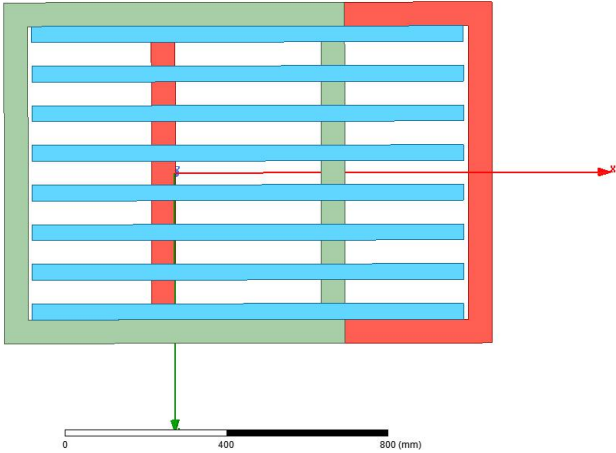

Figure 2.8: Bottom view of ferrite on transmitter side

The ferrite material used for the simulation has been taken from the company named 'Magnetics', who has a particular ferrite named as 'T material', which is to be used for the operation in 20kHz to 750kHz frequency range and since we are operating at 85kHz

frequency so this ferrite is the best available material to be used. The ferrite material properties are as shown in the Fig. 2.9 and the Table 2.2 below.
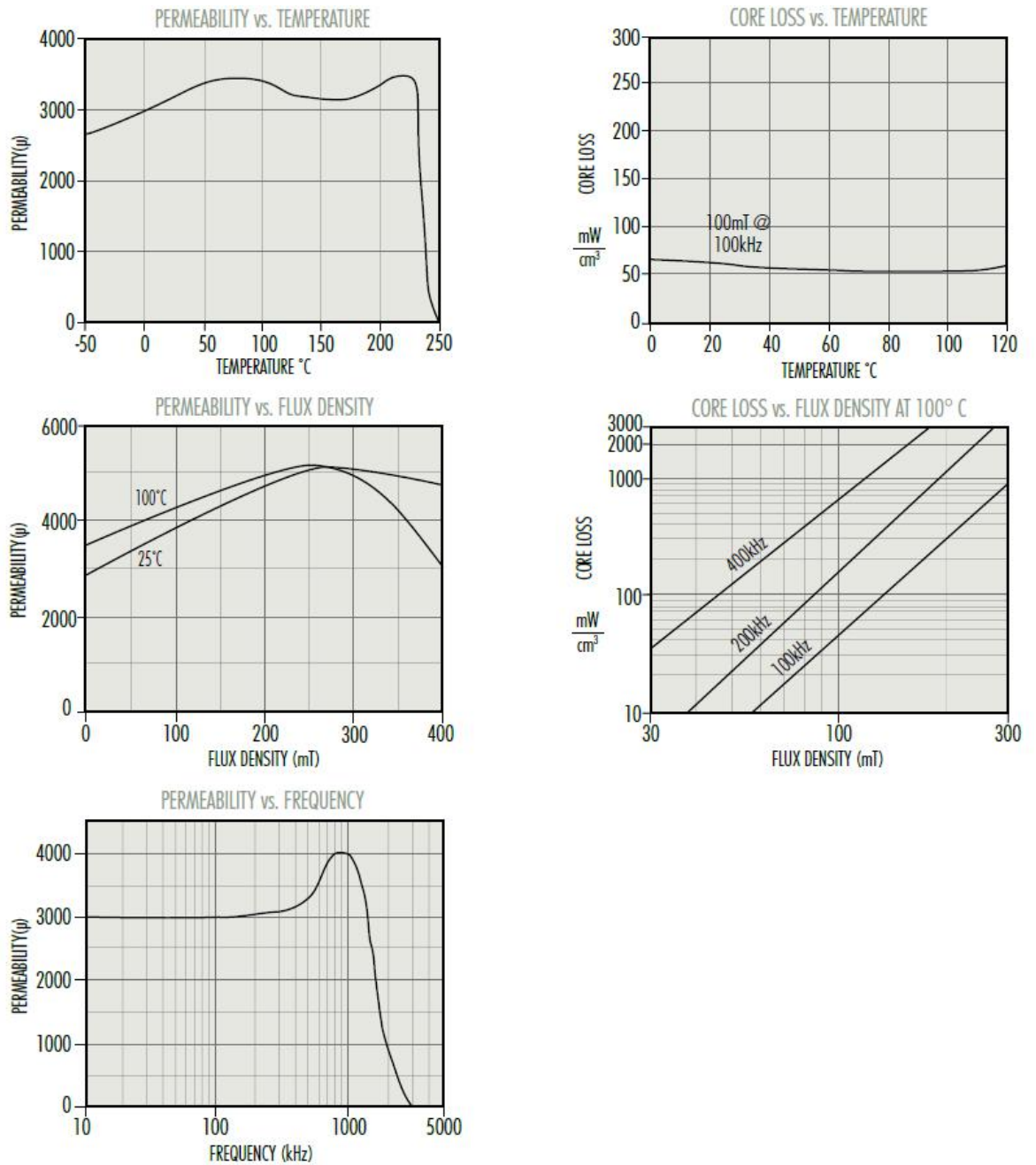

Figure 2.9: Typical properties of Ferrite model used

Number of Points	2
Number of curve	1
Length	1090mm
Width	40mm
Height	16mm
Initial Permeability	3000±25% at 25°C
Relative Permeability	Non Linear B-H curve
Relative Permittivity	12
Bulk Conductivity	0.2 siemens/m
Mass Density	4800 kg/m^3
Saturation Flux Density	0.53T at 11.9A.T/cm, 25°C
Area of each ferrite	123360mm^2
Volume of each ferrite	697600mm^3
Weight of each ferrite	3.34848 Kg

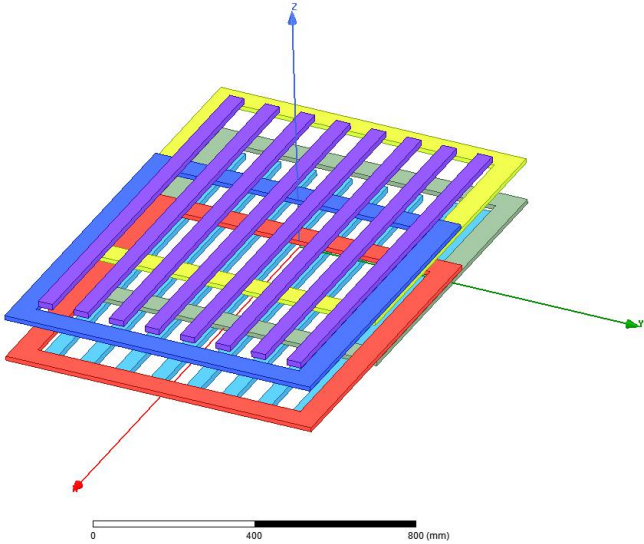*Table 2.2: Ferrite model properties*

Figure 2.10: View of the coils with the ferrites in place

2.4   Electromagnetic Shield Design

Since the magnetic fields are produced in all the directions we need to block the field which is in direction towards the inside of vehicle and also towards the ground else the human beings inside the car can be subjected to this electromagnetic field which can be dangerous and thus we need to shield the EM field on the direction which is not facing the transmitter and receiver. And hence for shielding we use the aluminium sheet to cover at the both transmitter and receiver end.

The aluminium shield is drawn using the function 'Draw Box', which is to create a 3D box which when given the thickness and shape can easily correspond as the EM shield. The details of the model is as shown in the Table 2.3 and the top view of the receiver side shield is as shown in the Fig. 2.11 below.

Length	1800mm
Width	1200mm
Height	4mm
Relative Permeability	1.000021
Relative Permittivity	1
Bulk Conductivity	38000000 siemens/m
Mass Density	2689 kg/m^3
Area of each shield	4344000mm^2
Volume of each shield	8640000mm^3
Weight of each shield	23.23296 Kg

Table 2.3: Aluminium model properties

As seen in the above Fig. 2.12 each of the section of the model is colour coded for easy identification of transmitter and receiver side coils,ferrites and shields. To keep the system close to practical world the system is designed inside a boundary consisting of air which envelops the entire model as seen in Fig. 2.12.
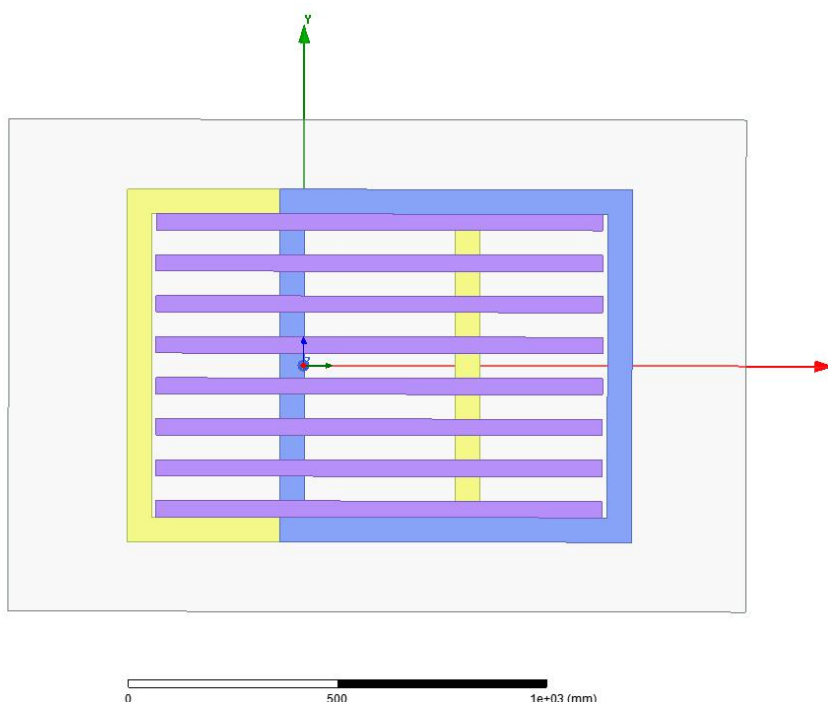
Figure 2.11: Top view of the shield as seen from receiver side of the coil

Length of each coil centre to centre	800mm in X axis
Width of the coil centre to centre	800mm in Y axis
Total length of Transmitter/Receiver coil in pair	1200mm in X axis
Overlap Distance between the coils centre to centre of the edge	375mm
Total Mass of the system on each side of Rx & Tx	91.184064 Kg

Table 2.4: Dimensions of the Transmitter and Receiver Coils

The Table 2.4 contains the information about the final dimension of the coil in transmitter and receiver side.
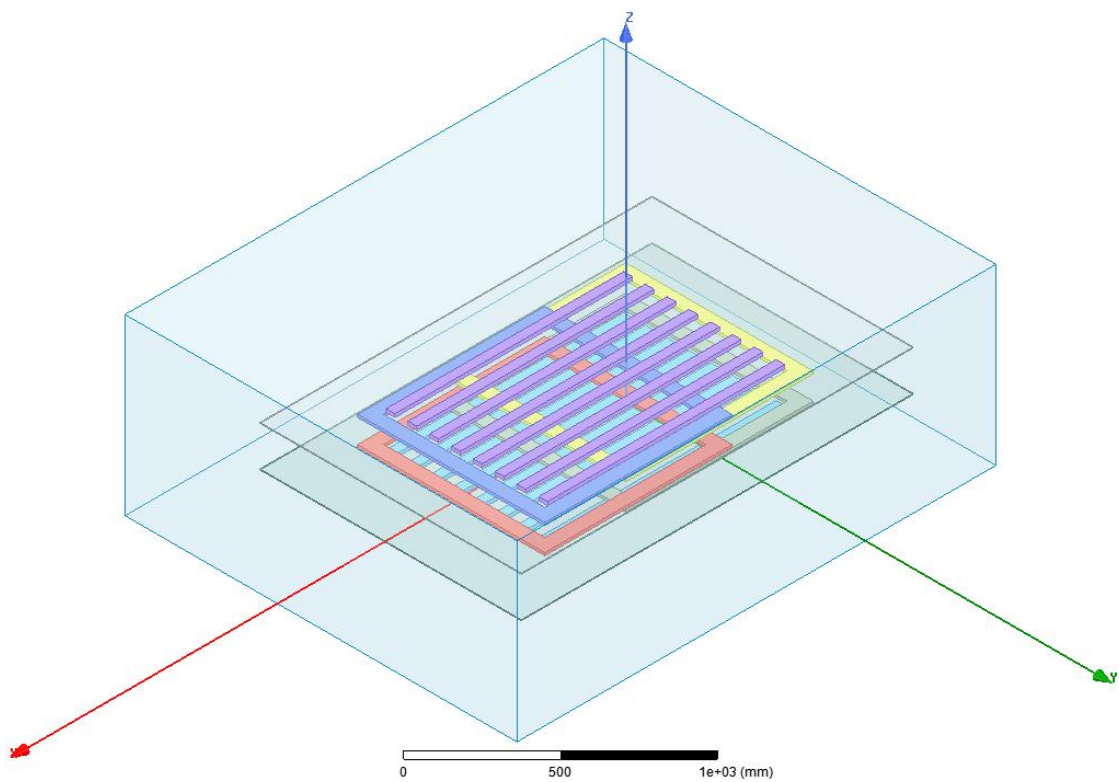
Figure 2.12: A view of the complete model for wireless power transfer, here the air is shown by the 3D box

Chapter 3

Magnetostatic Solution Setup

After designing of the model in ANSYS Maxwell 3D, we have to simulate our lumped model in each kinds of Magnetic solution type viz.
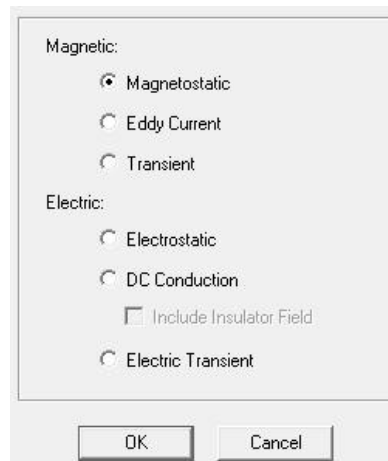
1. Magneto-static
2. Eddy Current
3. Transient

Figure 3.1: The solution type in Maxwell 3D, here showing magnetostatic is selected

We simulate our lumped model in each kind of magnetic solution and then this maxwell circuit is imported into simplorer in order to determine the efficiency, power transfer etc. with the power electronic circuit.

We will discuss in detail the setting up and the results of each type in the following chapters.

To set up the Ansys Maxwell 3D we use the project manager as shown in figure 3.2 for the following sections:

1. Boundary Condition

2. Excitation of the coils

3. Parameters to be calculated

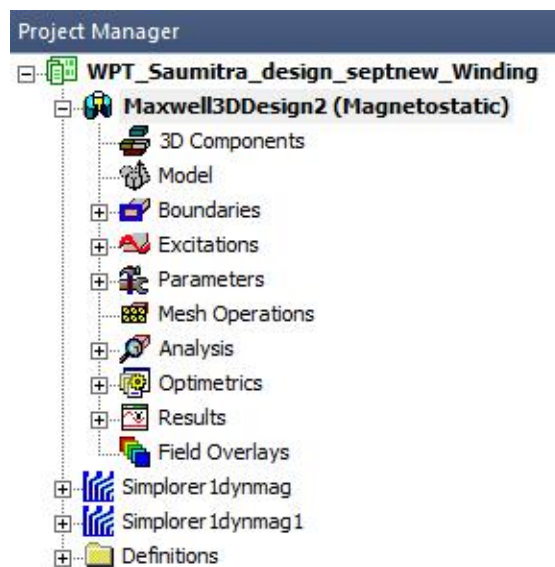4. Mesh Operation

5. Analysis

6. Optimetrics

Figure 3.2: Project Manager in Ansys Maxwell 3D in magnetostatic type

3.1 Boundary Condition

In order to run the simulation, the foremost step is to set up the boundary condition and here we setup the boundaries of each coil as *insulating* as the coils are overlapping each other on either side of transmitter and receiver so we need to use litz wire in practical scenario which has insulation. The visualization of insulation in the simulation can be seen in the figure 3.3 below.
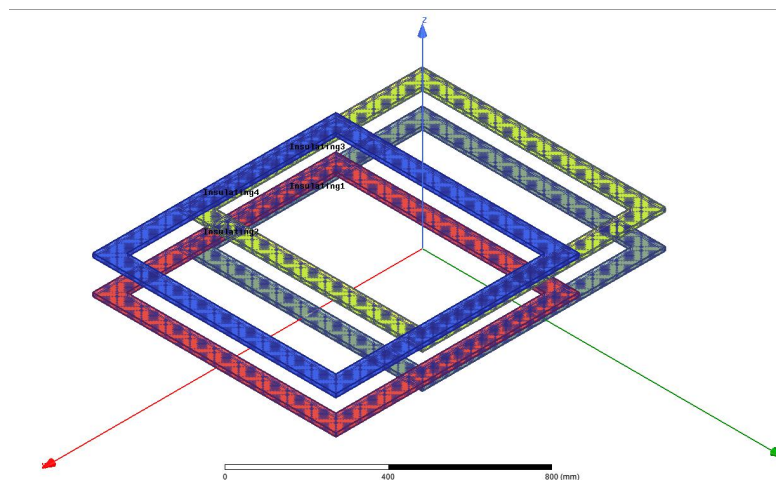
Figure 3.3: View of insulation in the coils used for simulation

3.2 Excitation of the coils

For excitation of coil in magnetostatic solution we need to apply current excitation in each coil winding in order to find the self and mutual inductance of the coil, hence the coupling coefficient can be found out here easily.
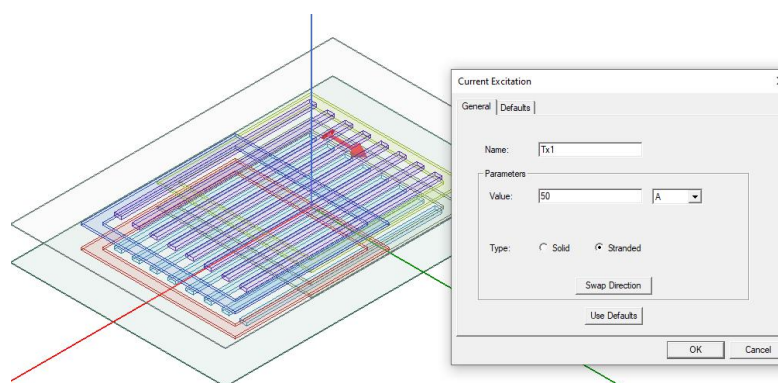

Figure 3.4: Excitation for transmitter coil1

Fig. 3.4 and Fig. 3.5 shows the excitation setup done in coil 1 and coil 4 respectively. Coil 1 being a transmitter coil is excited with 50 A of current and similarly for coil 2. Where as coil 3 and coil 4 being a receiver side coil is not excited with any current and thus its set as 0 A.
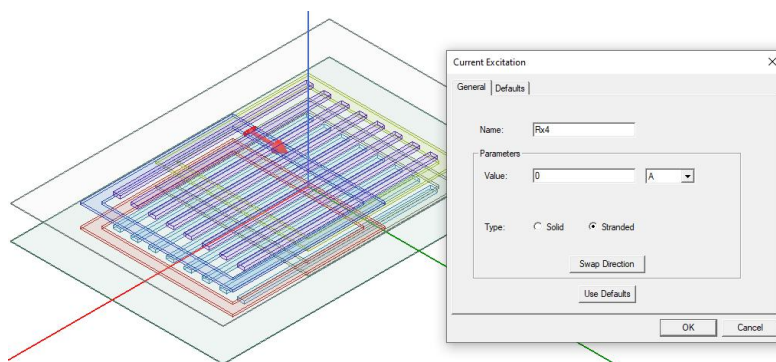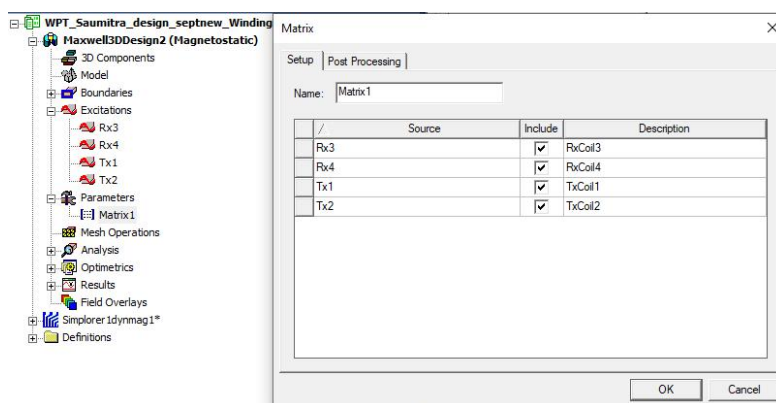
Figure 3.5: Excitation for receiver coil 4

Figure 3.6: Setup of parameters needed to be calculated

3.3   Parameters

As we need to calculate the inductance matrix and hence we include matrix as the parameter to be calculated as shown in figure 3.6.

And the post processing tab is used to setup the number of turns in the coil (which in our case is 5 turns) in this magnetostatic solution type as seen in figure 3.7.

3.4   Analysis

This is the setup where you set the system how it has to be solved like if it has to be converged after every pass, also the minimum error percentage in the solution can be set here and this can be seen in the figure 3.8. The convergence tab can be use to increase the refinement per pass which by default is set to 20%
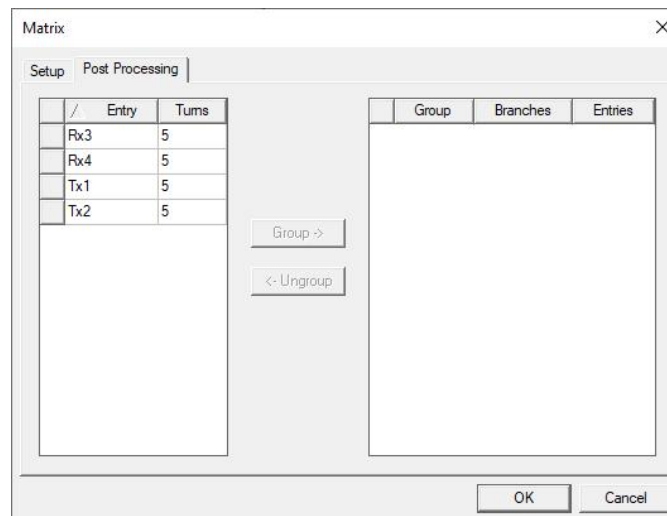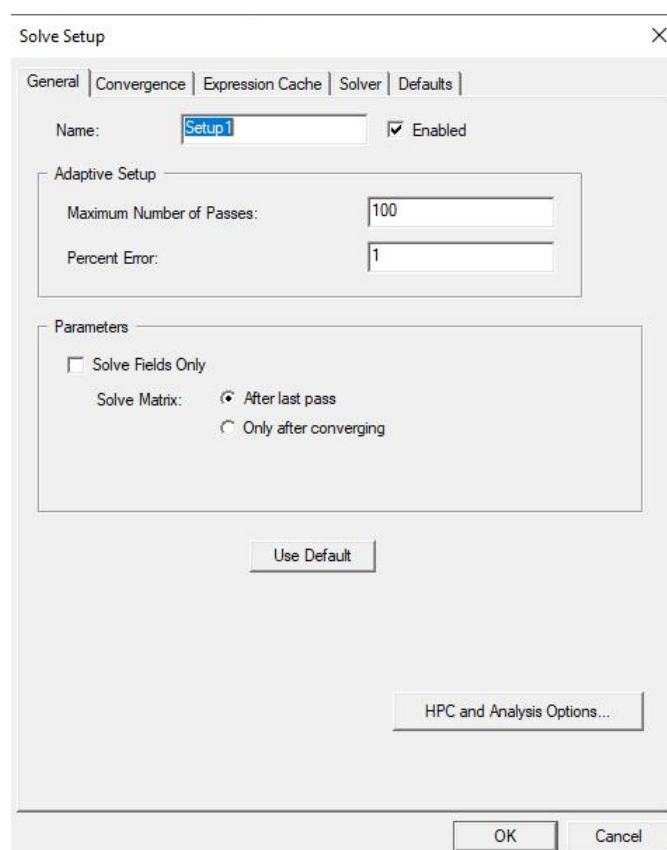
Figure 3.7: Setup of post processing tab

Figure 3.8: Setup used in magnetostatic solution

3.5   Optimetrics

This is used to setup a linear sweep required to measure the values at various steps of changing values. In this solution we setup to change the overlapping distance between the two coils of transmitter and receiver and try to find out the position in which both the coils in transmitter and receiver side mutually decoupled with each other respectively.

The figure 3.9 shows the setup that we used in this solution in order to find the overlap distance as discussed in 2.2.1.
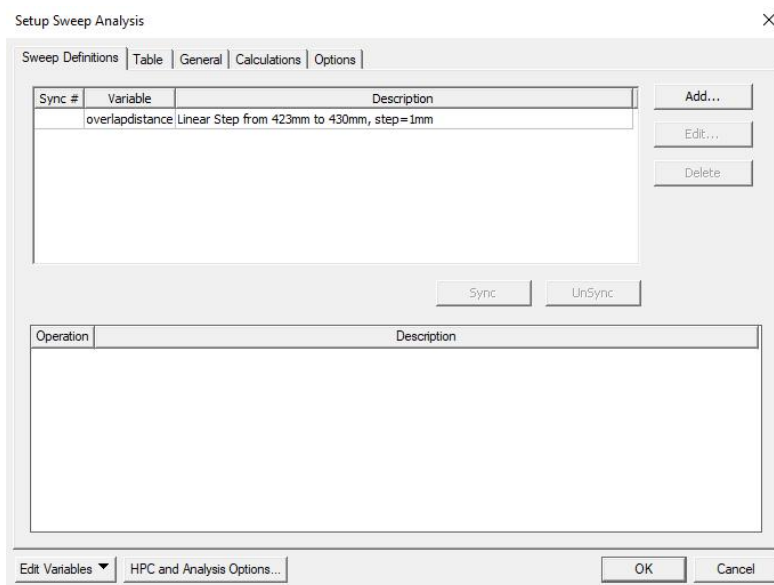

Figure 3.9: Overlap distance is varied here to find minimum coupling

And this is all needed to setup here in magnetostatic solution type which is mainly to find the mutual decoupling between the 2 coils in each side of trasnmitter and receiver. And then this setup is used further to setup as eddy current solution which will be our final setup for the results needed.

Chapter 4

Eddy Current Solution Setup

After the setup of magnetostatic solution as discussed in chapter 3 and the setup is executed we then transfer the magnetostatic solution into eddy current solution as in practical scenario we will have an AC current as input operating at a higher frequency and thus to calculate further we need to set up the system in eddy current solution type.

1. Boundary Condition
2. Excitation of the coils
3. Parameters to be calculated
4. Mesh Operation
5. Analysis
6. Optimetrics

4.1 Boundary Condition

This setup remains the same as discussed in chapter 3 so the insulation condition remains the same as seen in figure 3.3.

4.2 Excitation of the coils

As this is eddy current solution so here we setup the coil with winding and coil terminal where we can represent the number of turns by the number of conductors. Thus in our case we set number of conductors to 5 in each of the coils, and there are 4 windings in the
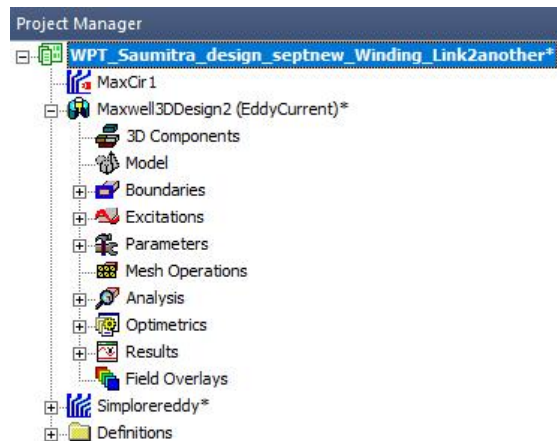
Figure 4.1: Project Manager in Ansys Maxwell 3D in eddycurrent type

total system each of them linked with the respective coil in the transmitter and receiver side and each winding is linked to its respective coil terminal excitation.

In this project we have named the transmitter side coil as Txcoil 1 and Txcoil 2 with windings Tx1 and Tx2 respectively having TxC1 and TxC2 as the respective coil terminal excitation.
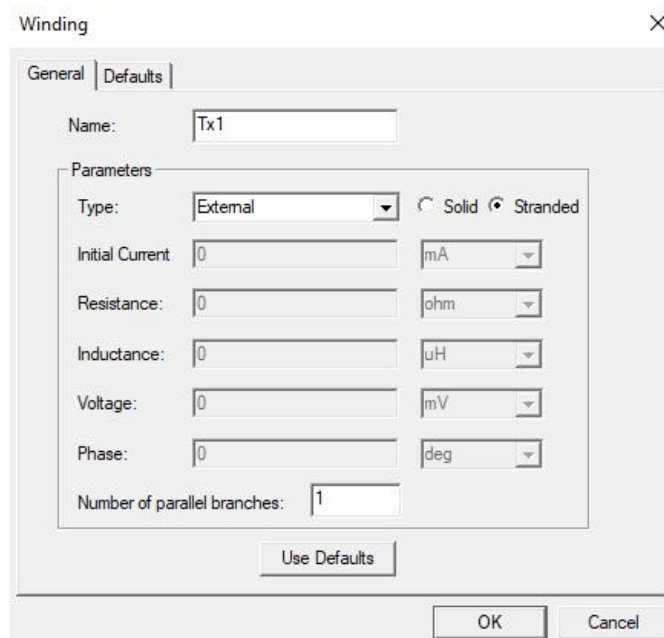

Figure 4.2: Configuration for TxCoil 1 winding

As seen in figure 4.2 the winding is set to type external so in this case we prepared
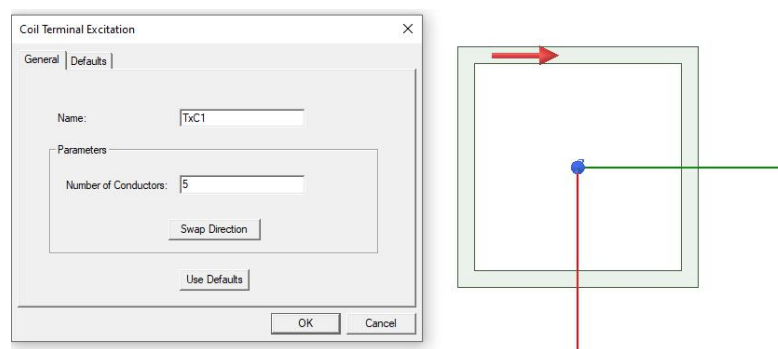
Figure 4.3: Tx1 Coil Terminal excitation setting with the direction of current in TxCoil1

an external circuit in the function named as 'Maxwell Circuit Design', which is as shown in figure 4.4 below.
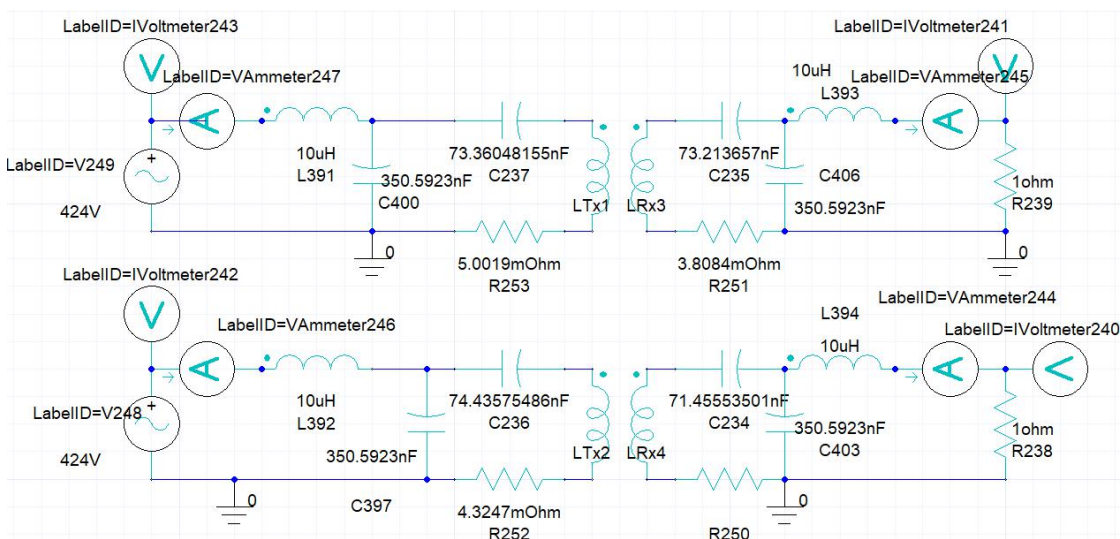

Figure 4.4: The circuit diagram which is used to simulate the coils for wireless power transfer along with LCC compensation

We can find from figure 4.4 that we have set the source supply voltage at 424V with a frequency at 85kHz supplied to Txcoil 1 and Txcoil 2, both are in phase with each other. Also LCC compensation is in place here where the values of capacitor Cf_1, Cf_2, Cf_3, Cf_4 and inductor Lf_1, Lf_2, Lf_3, Lf_4 are calculated as discussed in section 1.11 and the values are as shown in Table 6.1.

Here we have Rload 1 and Rload 2 representing the load of the system which in practical are the two battery systems kept separately in this case for easy simulation.

The equivalent resistance is calculated considering the Tesla Model S where the battery voltage is fixed at $V_{battery} = 350V$, the capacity to be 100kWh and considering the wireless power to be transferred as $P_{out} = 100kW$ we calculate the equivalent load resistance as in equation 4.1

$$R_{loadeqv} = \frac{V_{battery}^2}{P_{out}}$$

(4.1)

The calculated resistance occurs to be $R_{loadeqv} = 1.225\Omega$ and multiplying with the ratio $\frac{8}{\pi^2}$ which determines the equivalent resistance from DC side to AC side is nearly equal to 1Ω so hence we have 1Ω load for each of the coil which is for RxCoil 3 and RxCoil 4.

4.3 Parameters

This part remains the same as it was discussed in chapter 3 but in this case as we have mentioned the number of turns of the coil in the coil terminal excitation as said in section 4.2 and hence in the post processing tab the number of turns is left as 1 and not 5 as was in previous chapter 3.

4.4 Analysis

This setup is also similar to the one in chapter 3 but it has 2 tabs which needs to be set up as shown in figure 4.5 & figure 4.6 .

When all this two extra setup is done in this setup we can verify that all the conditions are correct and then we can start the analysis. The results of this analysis are discussed in chapter 5.

4.5 Optimetrics

As in chapter 3 in this case also we set up parametric file to run a linear sweep but in this case we check the variation of the results with regard to misalignment in X and Y axis which can occur due to misalignment in the parking. Also we simulate the result if different variation in Z axis as many vehicles have different ground clearance and hence
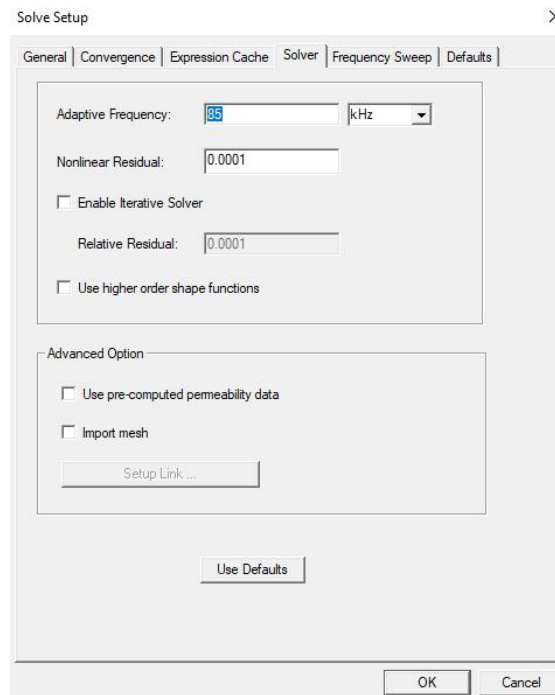
Figure 4.5: This tab we specify the working frequency of the system to determine results

the air gap can increase, so we need to find the maximum air gap that this system can transfer power efficiently.

The X and Y axis misalignment is taken form 0 mm to 400 mm in this optimetrics setup and the air gap is varied form 120 mm to 400 mm in order to find the coefficient of coupling
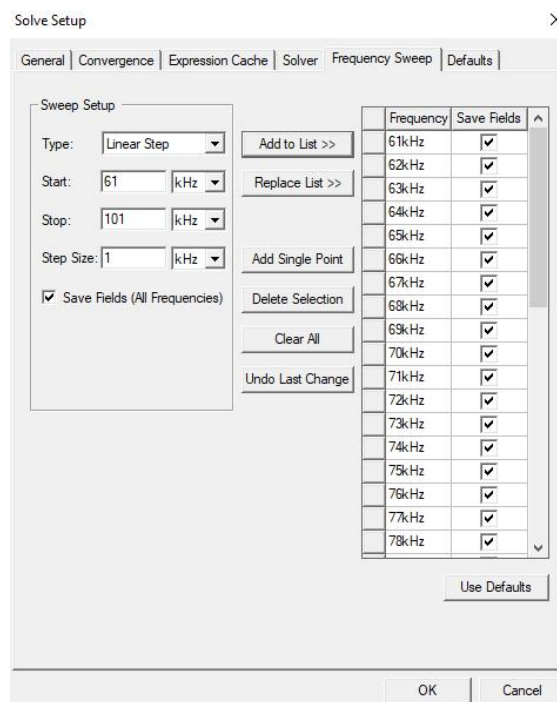
Figure 4.6: Frequency sweep tab to determine the function of the system in different frequencies

Chapter 5

Results and discussion of Maxwell 3D

5.1 Assumptions taken

The following assumptions/hypothesis has been used in order to arrive the results discussed in this chapter:

- The model designed here is a lumped model in comparison to the actual model to reduce the complexity of simulation.

- The Ferrite used here is designed as per the standard I block used as discussed in [19].

- Except ferrite the core loss is setup by the default of Ansys.

- The coil is enveloped in air as the boundary and is made up of Litz wire strands and hence eddy current effect is not considered

-

We will hereby discuss the results as obtained from eddy current setup which was discussed before for our model and is in deed as accurate as we need in real world situation.

47

5.2   Coupling Coefficient and misalignment

5.2.1   X axis misalignment

The following figure 5.1 shows the variation of coupling coefficient with the misalignment in x axis and we can see that even when the misalignment is about 300mm from the centre the coupling between coil Rx3 and coil Tx2 rises enough to enable the wireless power transfer and this case is considering there is no misalignment in Y axis and at an air gap of 120mm from the transmitter.
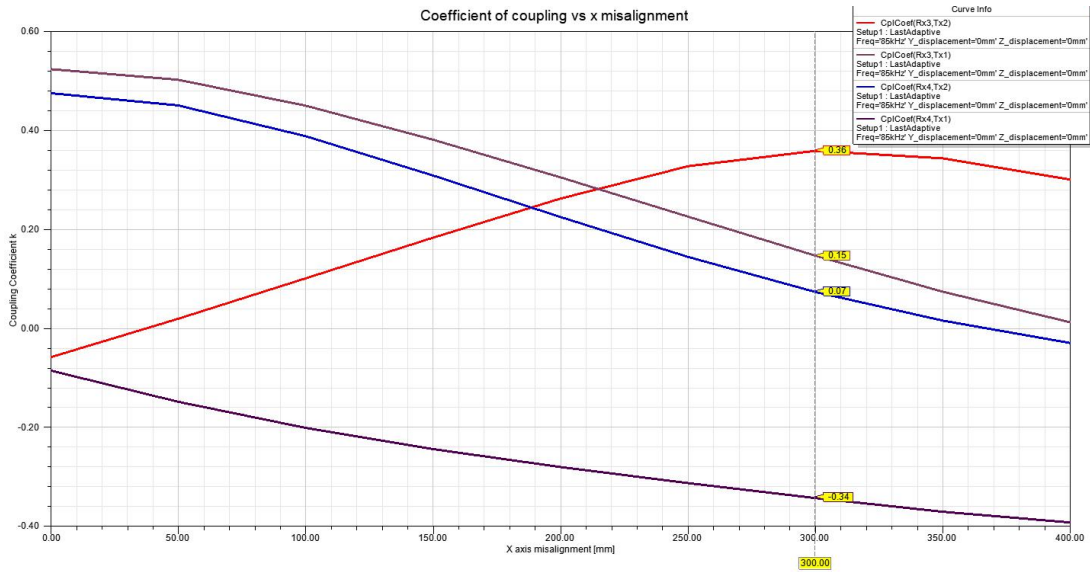

Figure 5.1: Coupling coefficient change with misalignment in X axis only

The Fig. 5.2 shows the values of coupling coefficient from the Fig. 5.1.

	X_displacement [mm]	CplCoef(Rx3,Tx1) Setup1 : LastAdaptive Freq='85kHz'	CplCoef(Rx4,Tx2) Setup1 : LastAdaptive Freq='85kHz'	CplCoef(Rx3,Tx2) Setup1 : LastAdaptive Freq='85kHz'	CplCoef(Rx4,Tx1) Setup1 : LastAdaptive Freq='85kHz'
1	0.000000	0.523310	0.474788	-0.058321	-0.085177
2	50.000000	0.501846	0.450069	0.019307	-0.148177
3	100.000000	0.449583	0.387985	0.100941	-0.200875
4	150.000000	0.380832	0.308550	0.183087	-0.243775
5	200.000000	0.304743	0.224677	0.262015	-0.279937
6	250.000000	0.225495	0.144209	0.327374	-0.312404
7	300.000000	0.146640	0.073338	0.358373	-0.342663
8	350.000000	0.073736	0.015492	0.343160	-0.370279
9	400.000000	0.012175	-0.029720	0.300186	-0.391926

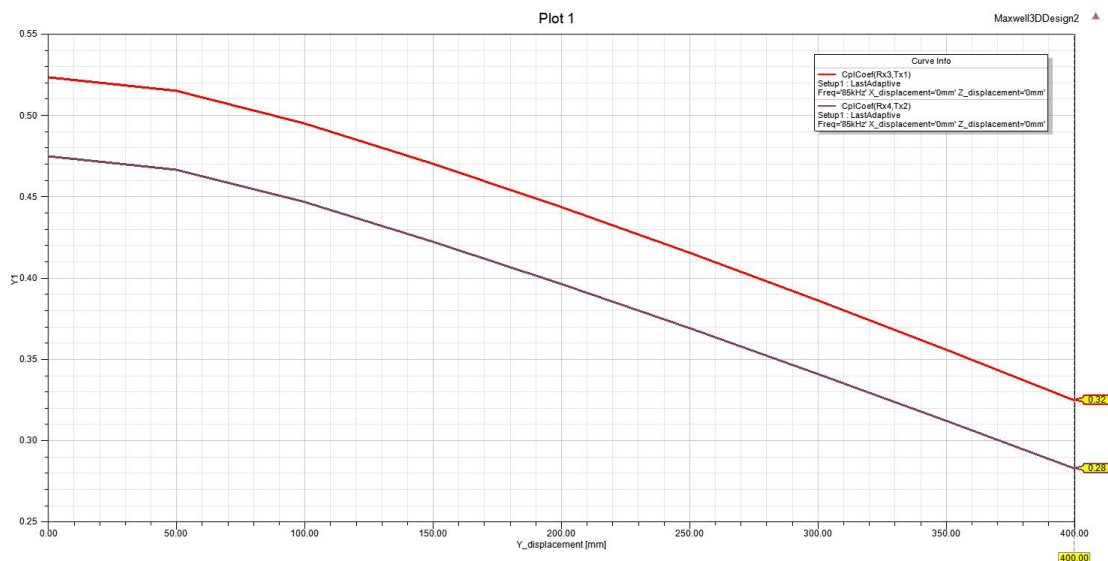Figure 5.2: Values of coupling coefficient in X axis misalignment

Figure 5.3: Coupling coefficient change with misalignment in Y axis only

	Y_displacement [mm]	CplCoef(Rx3,Tx1) Setup1 : LastAdaptive Freq='85kHz' X_displacement='0mm'	CplCoef(Rx4,Tx2) Setup1 : LastAdaptive Freq='85kHz' X_displacement='0mm'
1	0.000000	0.523310	0.474788
2	50.000000	0.515005	0.466496
3	100.000000	0.494908	0.446665
4	150.000000	0.470118	0.422211
5	200.000000	0.443536	0.396256
6	250.000000	0.415437	0.369127
7	300.000000	0.386122	0.340887
8	350.000000	0.355802	0.312144
9	400.000000	0.324597	0.282789

Figure 5.4: Values of coupling coefficient in Y axis misalignment

5.2.2   Y axis misalignment

The following figure 5.3 shows the misalignment only in Y axis i.e. when air gap is at 120mm and x axis misalignment is zero and we can see that even after a misalignment of 400mm the coupling coefficient is reduced only till 0.28 and 0.32 and hence still will be able to transfer power as the minimum coupling required is about k=0.10 [8].

The table 5.4 shows the values of coupling coefficient from the figure 5.3.

5.2.3   Z axis misalignment/ Difference in air gap

The following Fig. 5.5 and the Table 5.1 shows the reduction in coupling coefficient when the air gap between the coil is increased from 120mm to 400mm and having no misalignment along x and y axis.
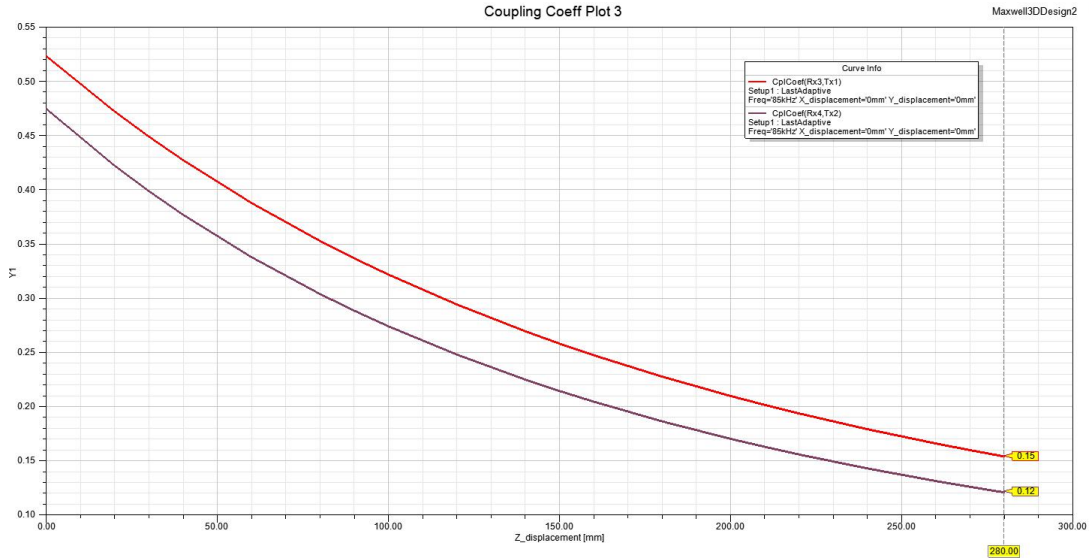

Figure 5.5: Coupling coefficient with change in air gap ie z axis

Z_displacement [mm]	Actual Air Gap	CplCoef(Rx4,Tx2)	CplCoef(Rx3,Tx1)
0	120	0.474788	0.52331
20	140	0.422262	0.472223
40	160	0.376983	0.427362
60	180	0.337853	0.387773
80	200	0.30389	0.352791
100	220	0.274069	0.321761
120	240	0.248006	0.294168
140	260	0.2249	0.26948
160	280	0.204572	0.24733
180	300	0.186407	0.227624
200	320	0.170278	0.209752
220	340	0.155878	0.193661
240	360	0.142976	0.179134

Z_displacement [mm]	Actual Air Gap	CplCoef(Rx4,Tx2)	CplCoef(Rx3,Tx1)
260	380	0.131378	0.165944
280	400	0.120875	0.154004

Table 5.1: Table showing the values of coupling coefficient from the Fig. 5.5

5.3 Ferrite core saturation

To find out if at this power level the ferrites are working in the saturation region or within its saturation limit of 0.3 Tesla we plot the complex magnitude of magnetic flux density B in ferrites both in transmitter and receiver side as seen in Fig. 5.6, 5.7 and Fig. 5.8, 5.9 and we can see that the maximum flux density is about 0.19956 Tesla which is within the limit of saturation.
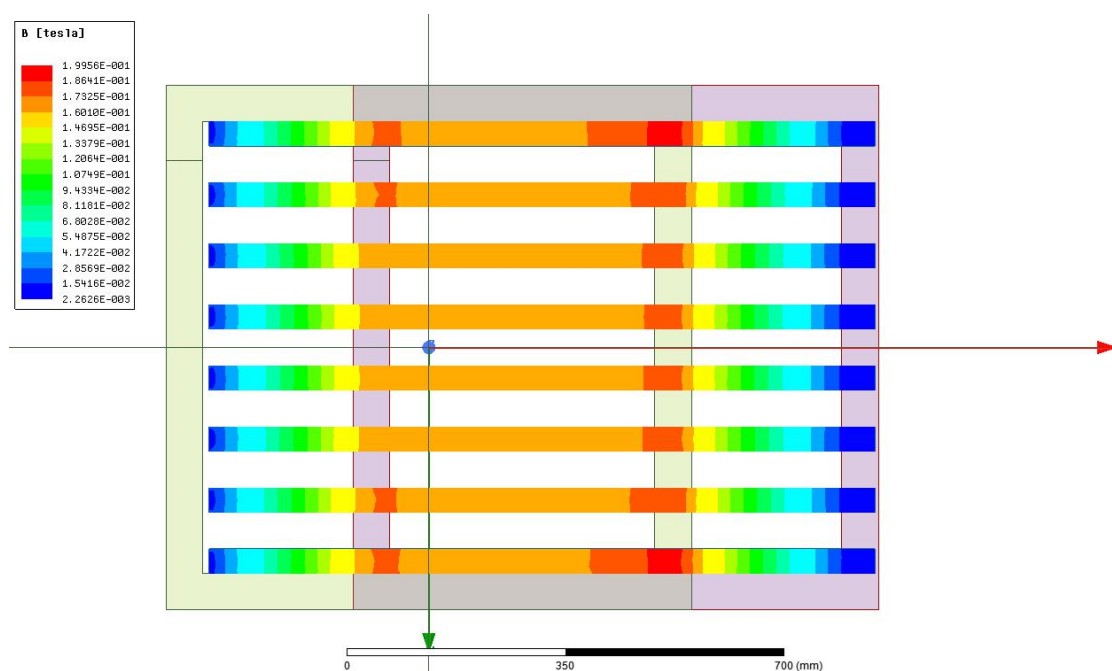
Figure 5.6: Complex magnitude of magnetic flux density in transmitter side ferrites

From Fig . 5.6 and Fig. 5.8 we can easily understand that the ferrites in transmitter side has higher magnetic flux density than the ferrites in receiver side and since they are within their saturation limit we can say it is a good model.
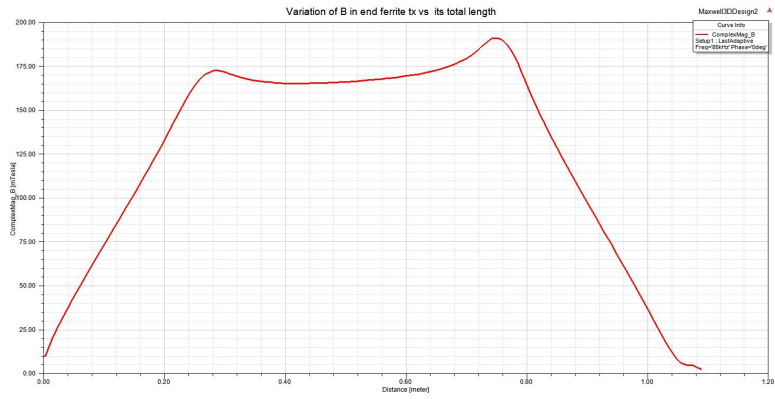
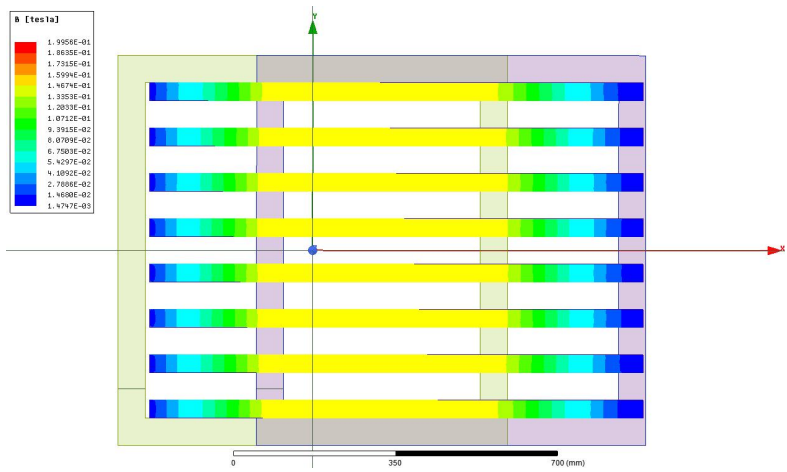Figure 5.7: Variation of complex magnitude B inside end ferrite Tx vs its total length

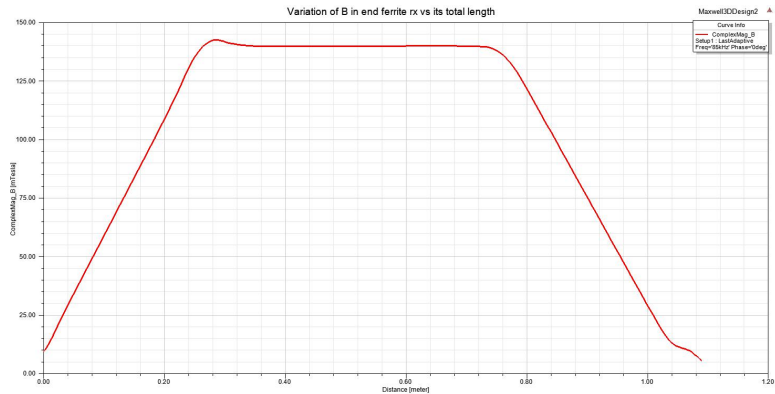Figure 5.8: Complex magnitude of magnetic flux density in receiver side ferrite

Figure 5.9: Variation of complex magnitude B inside end ferrite Rx vs its total lenth

5.4 Magnetic Field Intensity

The magnetic field intensity is calculated through a cut section placed in the centre of the coil and the Fig. 5.11 shows the complex magnitude of magnetic field intensity in that region of air the maximum being 4600A/m . And Fig. 5.10 shows the vector of magnetic field intensity at phase 90°.
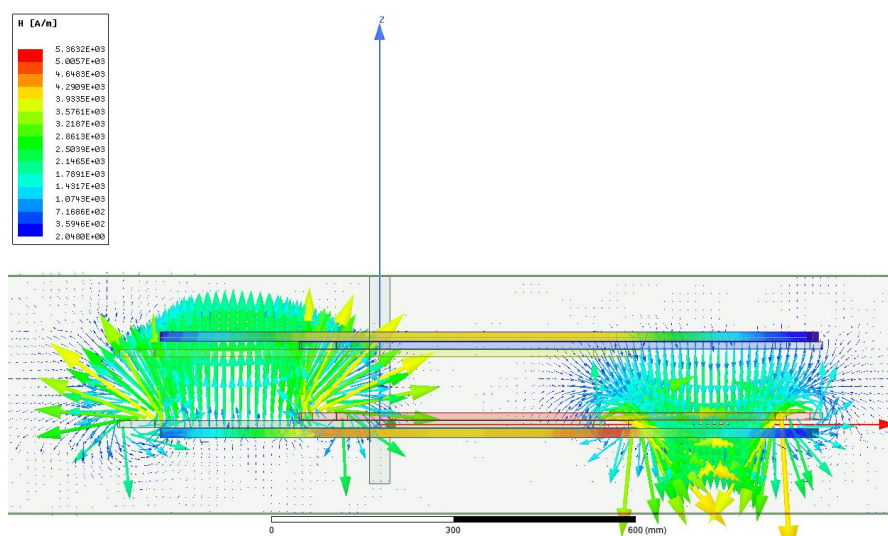

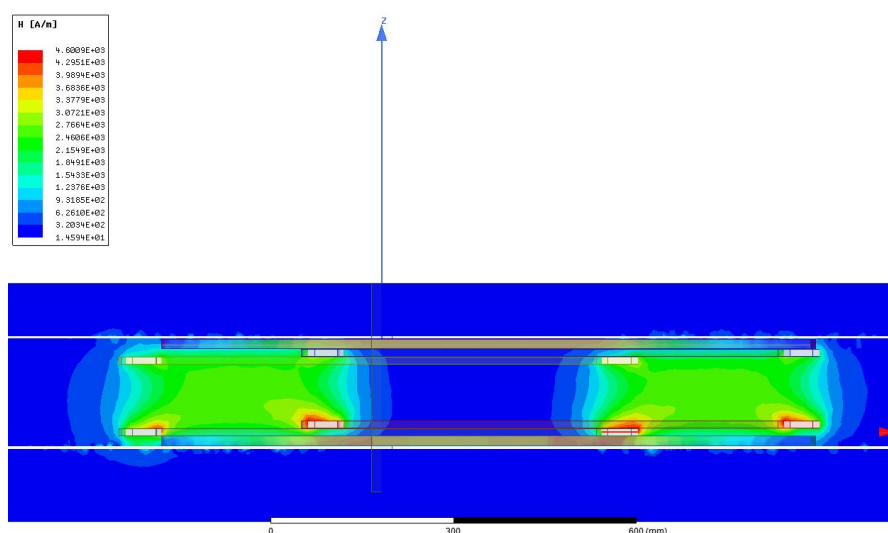Figure 5.10: Vector view of magnetic filed intensity at 90°

Figure 5.11: Complex magnitude of magnetic field intensity

5.5   Magnetic Flux Density

The magnetic flux density is plotted in the same manner using a cut section in the coil and we can find in Fig. 5.12 the complex magnitude of the magnetic flux density in the region of transmission.
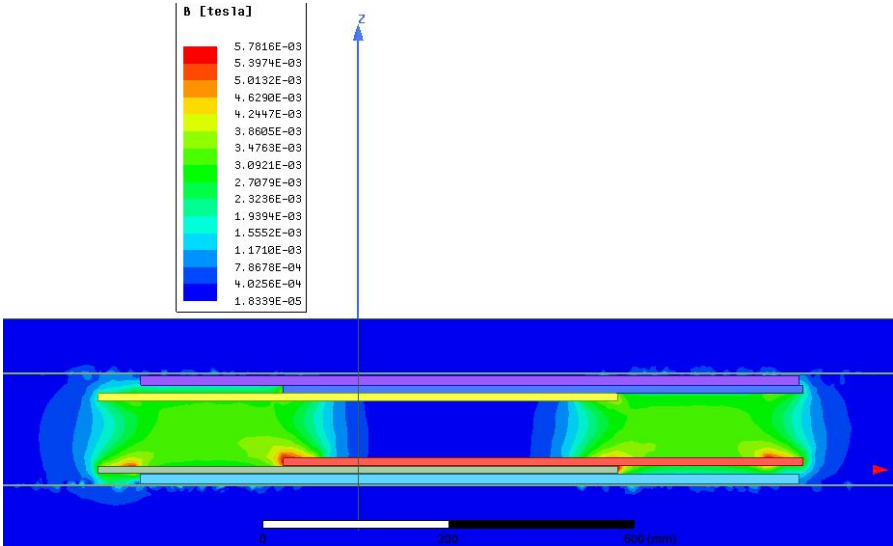

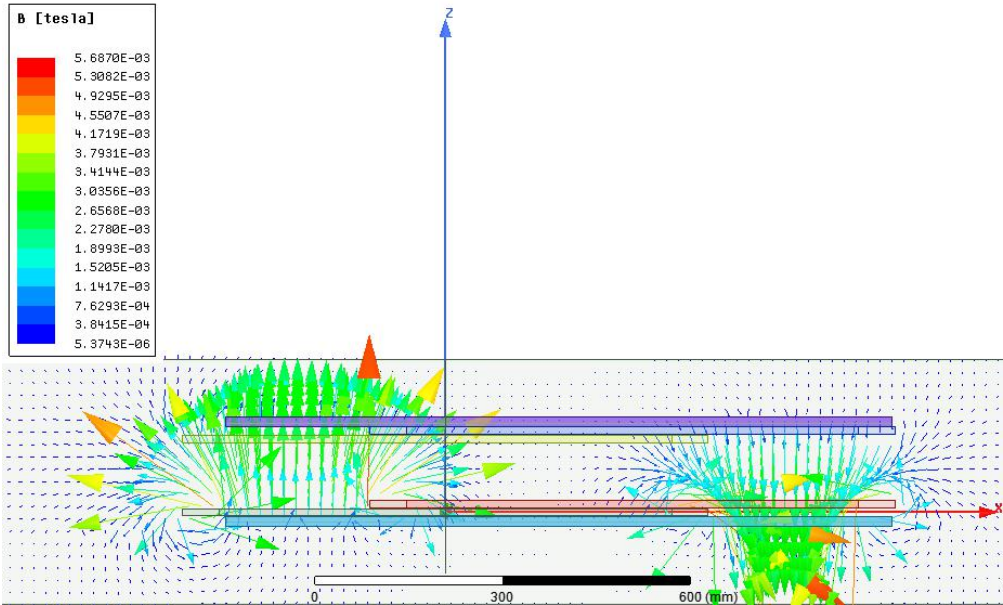*Figure 5.12: Complex magnitude of magnetic flux density in air*

Figure 5.13: Vector view of magnetic flux density at 90 °.

5.6 Current Density in coils

The complex magnitude of current density in the coils can be seen in Fig. 5.14 the maximum being 0.56986 A/mm^2 and minimum being 0.03799 A/mm^2 which is much below of the maximum limit of 4 A/mm^2.
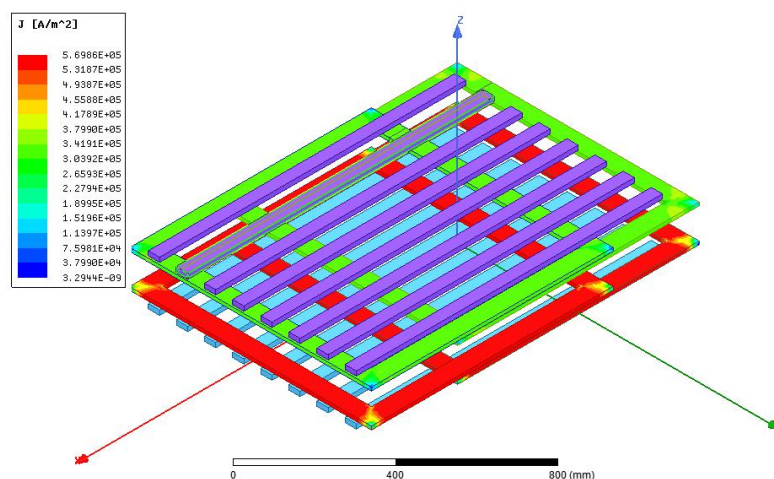

Figure 5.14: Complex Magnitude Current Density in Tx and Rx coils

5.7 Hysteresis Loss in the shield

The following Fig. 5.15 shows the hysteresis loss in the aluminium shield and we can determine easily that the losses are mostly in the yellow colored region which is in the range of 6.67E-12 W/m^3 to -3.054E-11 W/m^3.
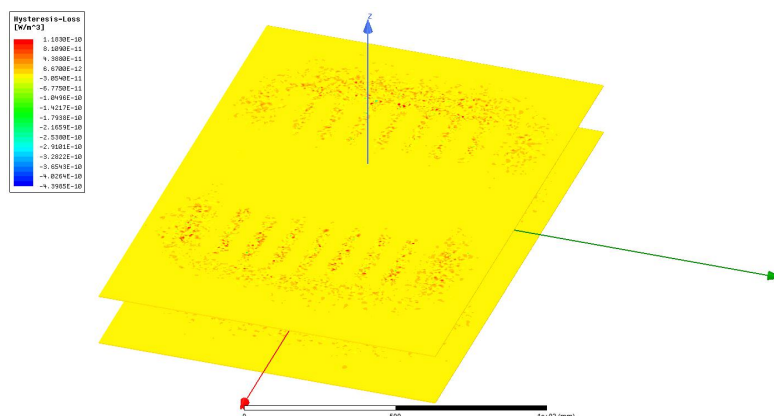

Figure 5.15: Hysteresis loss in the aluminuim shield

5.8 Core Loss

The core loss in the ferrites are calculated as mentioned in the section 2.3 where the values are derived from the data sheet and implemented in the Ansys to calculate the losses. The values are in the range 1.7336E05 W/m^3 to 1.1559E04 W/m^3.
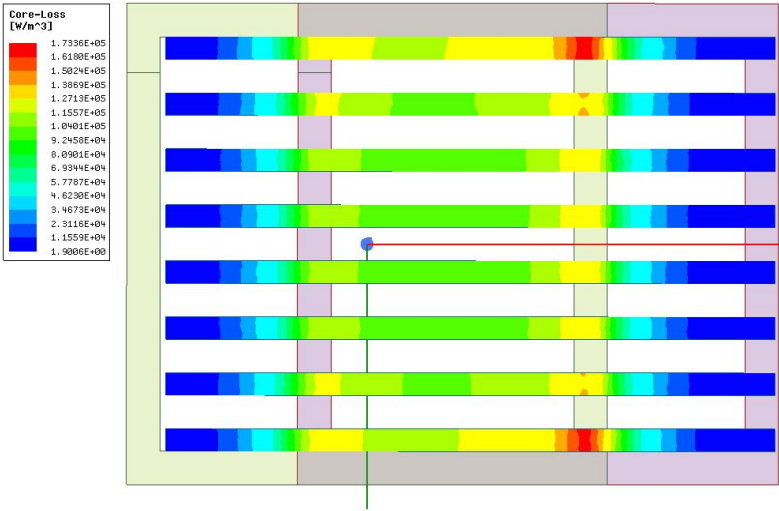

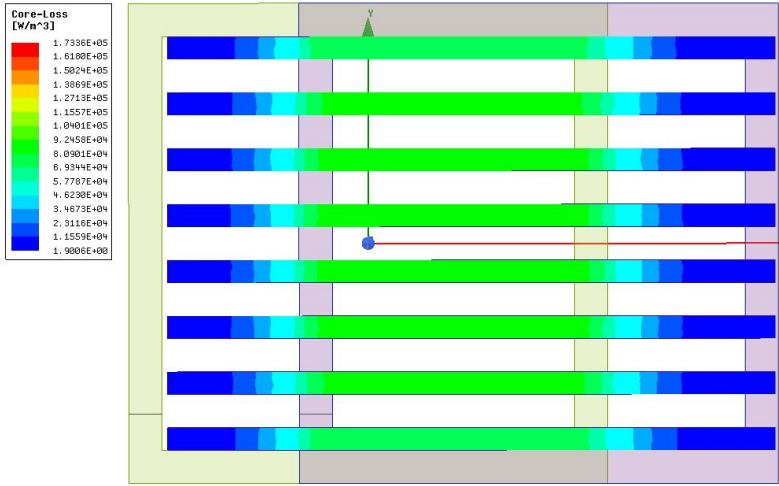Figure 5.16: Core loss in the ferrites of transmitter coil side

Figure 5.17: Core loss in the ferrites of receiver coil side

5.9 EM Loss in the whole system

The Fig. 5.18 shows the EM loss in the shield and ferrites. In the top view the reciever side shiled EM losses is omitted in order to get a view of the ferrites and the loss is similar to the transmitter side shield which is in Fig. 5.19.
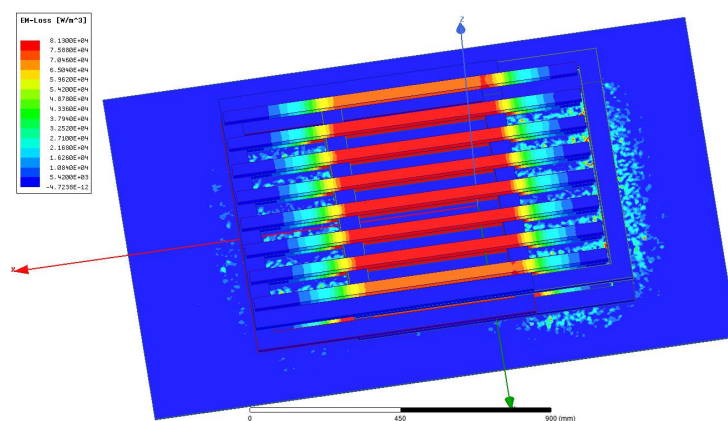

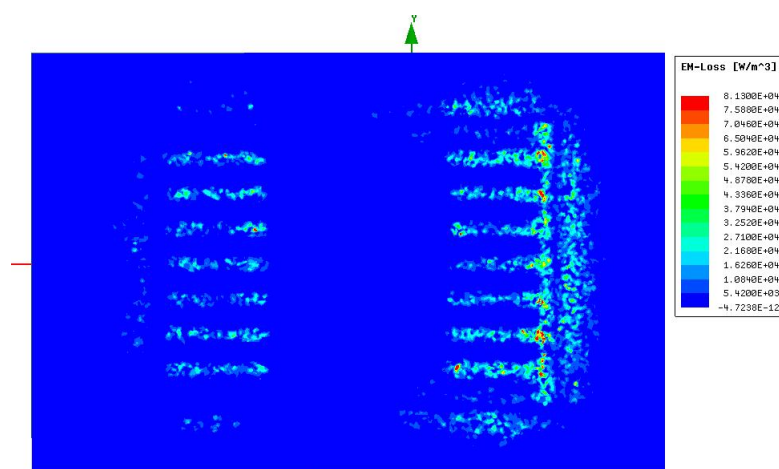Figure 5.18: EM loss in the enire system (without Rx shield)

Figure 5.19: EM loss in the Tx side shield

Part II

Ansys Simplorer

Chapter 6

Ansys Simplorer Setup

As discussed in chapters 3 and 4 we take the dynamic magnetostatic and dynamic eddy current circuit respectively into simplorer in order to simulate the electronic circuit of our system.

6.1   Import of Maxwell circuit and simplorer circuit setup

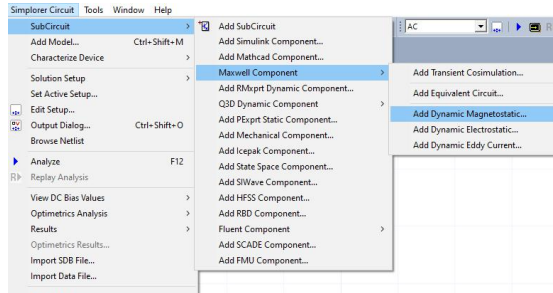So in order to import the circuit we follow as shown in figure 6.1 .

Figure 6.1: Way to import dynamic magnetostatic circuit

Notice the figure 6.2 and figure 6.4 both of which looks similar only that the magnetostatic equivalent circuit is named as LMatrix and eddy current equivalent is named as MxSS (where SS means Steady State) and thus we then connect this to the entire simulation circuit as shown in figure 6.3.

The values of capacitor Cf_1, Cf_2, Cf_3, Cf_4, also $CTx_1, CTx_2, CTx_3, CTx_4$ and inductor Lf_1, Lf_2, Lf_3, Lf_4 are calculated as discussed in section 1.11, these values are mentioned in table 6.1.
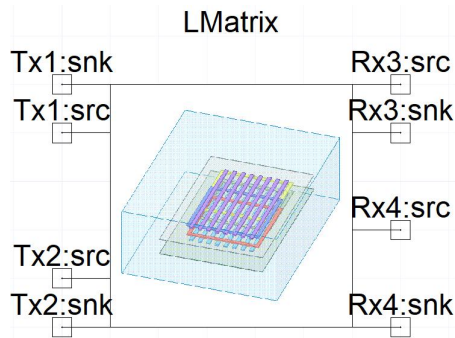
Figure 6.2: Equavalent magnetostatic ciruit in Simplorer
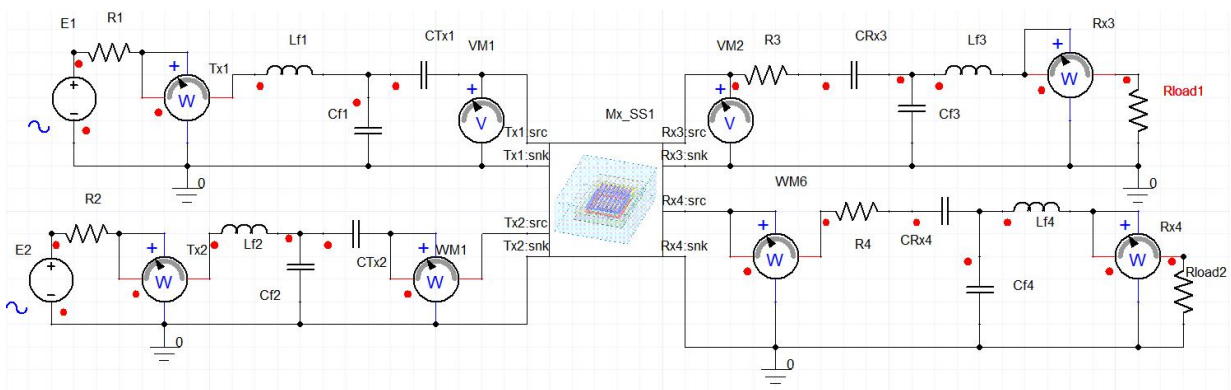

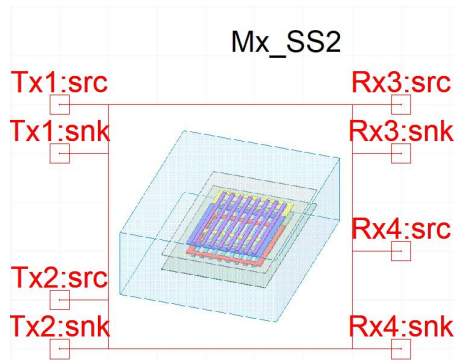Figure 6.3: The entire circuit in simplorer in eddy current setup

Figure 6.4: Equivalent eddy current circuit in simplorer

Parameter	Value	Parameter	Value
LTx1	57.79 µH	Lf1	10 µH
LTx2	57.099 µH	Lf2	10 µH

LRx3	57.886 µH	Lf3	10 µH
LRx4	59.064 µH	Lf4	10 µH
CTx1	73.361 nF	Cf1	350.5923 nF
CTx2	74.435 nF	Cf2	350.5923 nF
CRx3	73.214 nF	Cf3	350.5923 nF
CRx4	71.455 nF	Cf4	350.5923 nF
E1	400V @85kHz	E2	400V @85kHz
$Rload_1$	1 Ohm	$Rload_2$	1 Ohm

Table 6.1: Table showing the values used for circuit setup

The resistor R1,R2,R3 and R4 are added in order to add the coil resistance into this Simplorer circuit.

6.2 Analysis Setup

The analysis of Ansys Simplorer consist of AC(Frequency Sweep) and TR(Transient) and we need both this setup in order to obtain the results in time and frequency domain.

6.2.1 AC Analysis

The figure 6.5 shows the frequency sweep which we setup in the Simplorer for simulation and in this case from 1KHz to 1 MHz and this is used to find the efficiency of the system at different operating frequency. The AC sweep type is set as decadic with 500 points per decade in order to get a smooth cure for every points. The result obtain in this analysis is discussed in chapter 7.

6.2.2 TR Analysis

The figure 6.6 shows the setup for transient analysis which is chosen to show up to 1000 µs as after this duration the waveform is repeated so in order to have a better look at the waveform the end time is chosen as such.
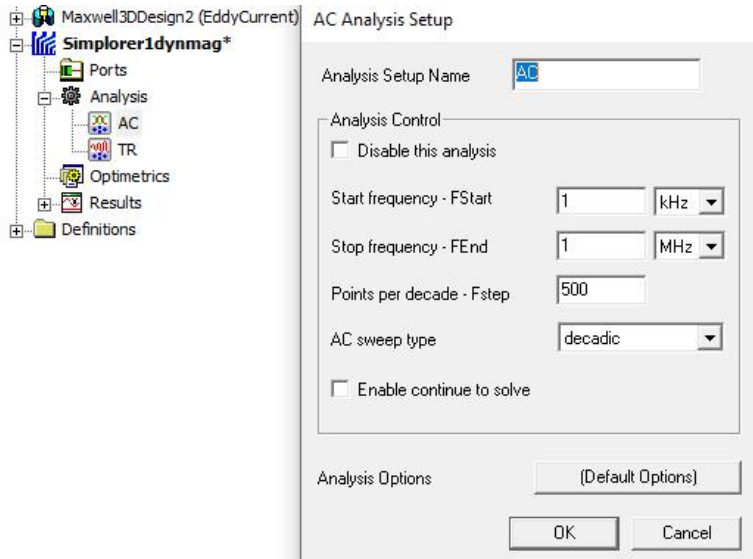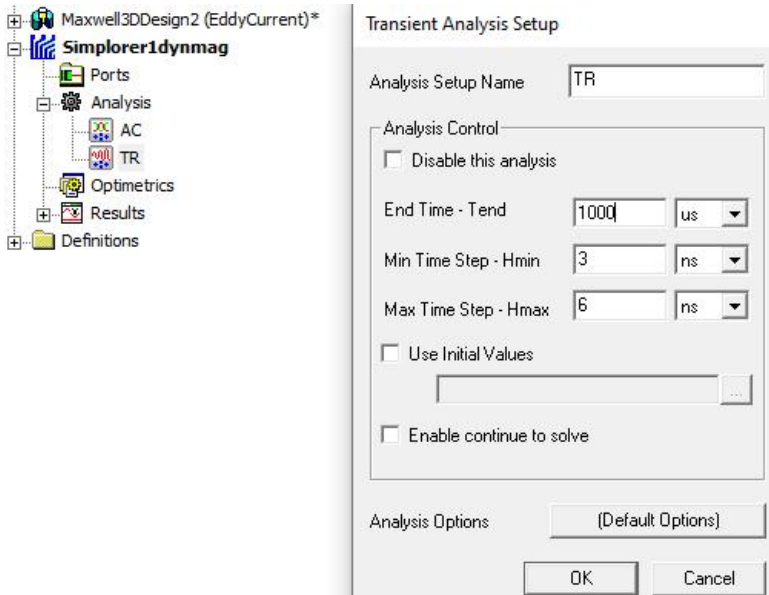
Figure 6.5: Frequency sweep setup

Figure 6.6: Transient Analysis setup

6.3   Optimetrics

This section is used to setup the values of misalignment that can occur in X,Y & Z axis direction and hence find out the amount of power that can be transferred due to the issues of misalignment.

Chapter 7

Results and discussion of Ansys Simplorer

As discussed in chapter 6 we have done two kind of analysis one being AC analysis and the other one is TR analysis. The AC analysis is a frequency sweep analysis used to find the behaviour of the system such as efficiency at different frequency of operation. The TR analysis is a transient analysis which shows the behaviour of the system with time i.e. from transient state to steady state.
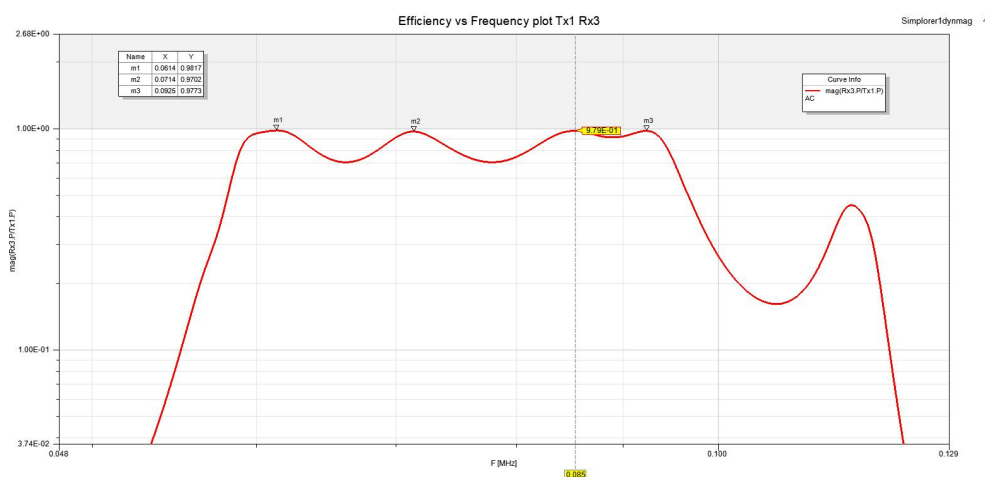
7.1   AC analysis results

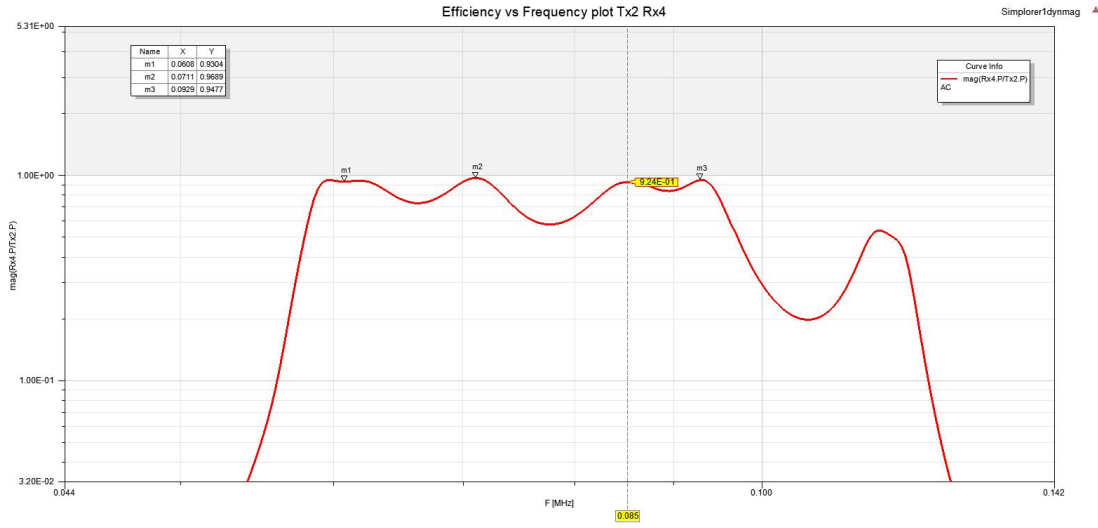*Figure 7.1: Efficiency vs Frequency of Tx1 and Rx3 coil*

Figure 7.2: Efficiency vs Frequency of Tx2 and Rx4 coil

In Fig. 7.1 and Fig. 7.2 we plot the Y axis as the Magnitude of ($\frac{Received power}{Transmitted power}$) and X axis being the frequency of operating the system. We have plotted four points where the efficiency is more than 90% along the frequency and hence the LCC compensation is reason for this behaviour, else we are supposed to find higher efficiency at just the frequency of resonance (here 85Khz) only. So use of LCC has been very beneficial for this kind of system where we can have higher efficiency even for operating at frequency other than resonant frequency.

7.2 TR analysis results

As we ran the TR analysis for 1000 µs we can easily find the transient state for the time period less than 400 µs, after which we see the steady state occurrence for the rest of the period and hence we calculate the RMS of the power, voltage during the steady state period and exclude the transient period.

7.2.1 Power Transferred

The RMS value and the efficiency from Fig. 7.3 & 7.4 is shown in the Fig. 7.5, values are in Watts.

Hence the total power from transmitter side is 46258.75W + 35517.74W = 81776.49W and the total power received in the receiver side is 45172.45W + 32854.73W = 78027.18W
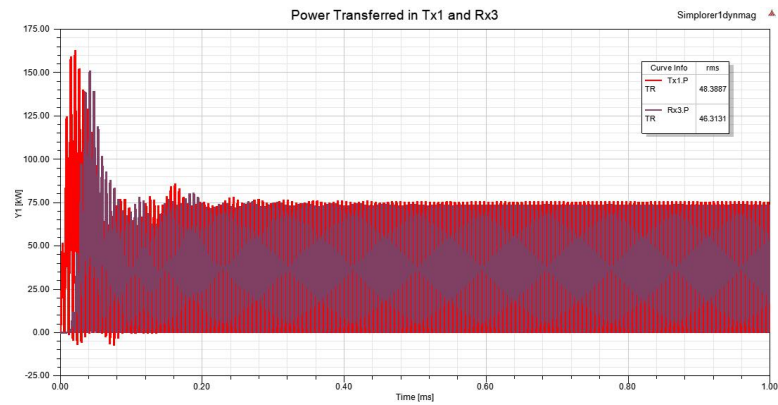
Figure 7.3: Power curve of Tx1 and Rx3
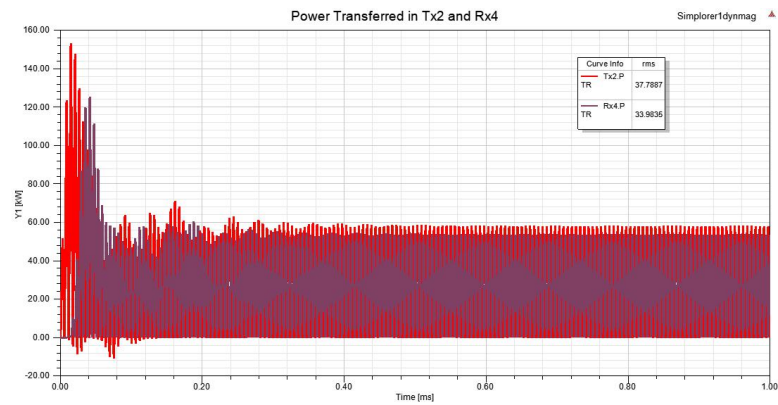
Figure 7.4: Power curve of Tx2 and Rx4

and thus the efficiency of the total power transferred is 94.42% which is in accordance with the assumptions taken before for the source and load.

rms(Tx1.P) TR	rms(Rx3.P) TR	rms(Tx2.P) TR	rms(Rx4.P) TR	rms(Rx3.P)/rms(Tx1.P) TR	rms(Rx4.P)/rms(Tx2.P) TR
46258.742795	45172.453765	35517.733179	32854.730326	0.976517	0.925023

Figure 7.5: RMS value of power transferred and received in the system with efficiency

7.2.2 Voltage
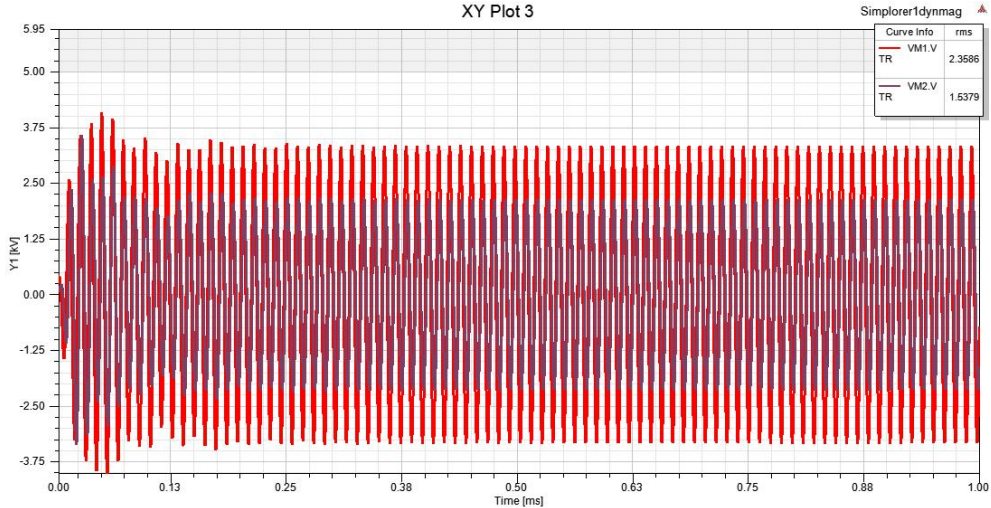
Figure 7.6: Voltage Across the coils of Tx1 and Rx3

Fig. 7.6 shows the voltage which is implemented in the coils after the compensation network. Fig. 7.7 & Fig. 7.8 shows the voltage which is measured by the watt meter placed in the circuit in Ansys Simplorer thus this is the source and load voltage measured in the circuit which is around 399V RMS and 190V RMS respectively.

Figure 7.7: Voltage measured in watt meter in Tx1 source and Rx3 load side

Figure 7.8: Voltage measured in watt meter in Tx2 source and Rx4 load side

7.2.3 Current

Figure 7.9: Current measured across the coil terminals of Tx2 (red) and Rx4(blue)

The values in Fig.7.9 are 75A RMS and 31.89A RMS for Tx2 and Rx4 respectively.

Conclusion

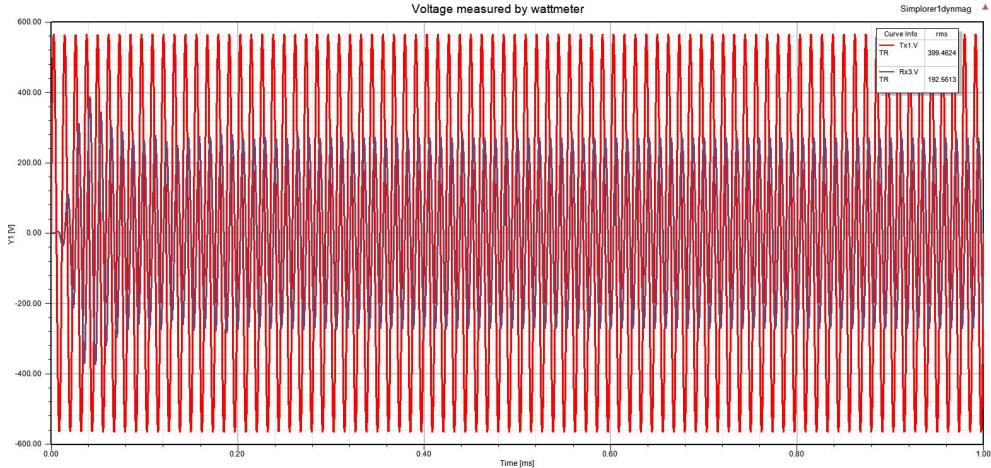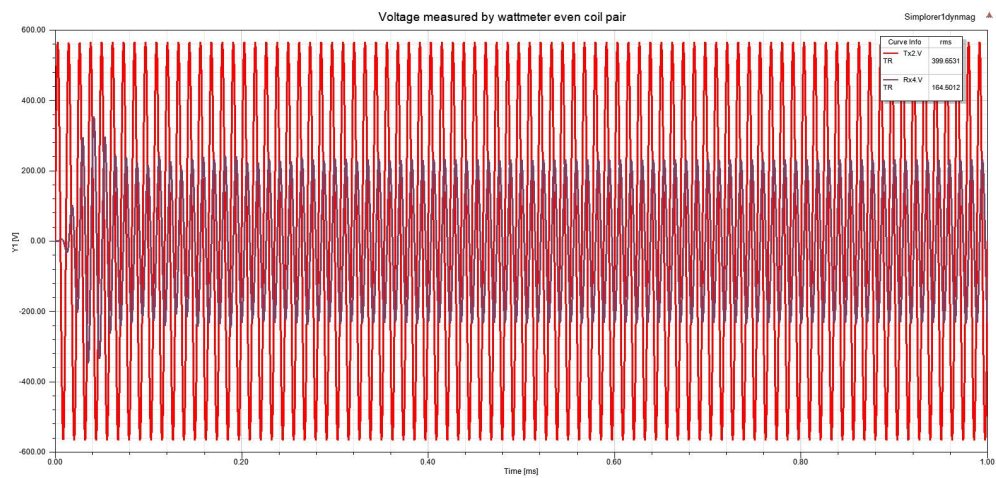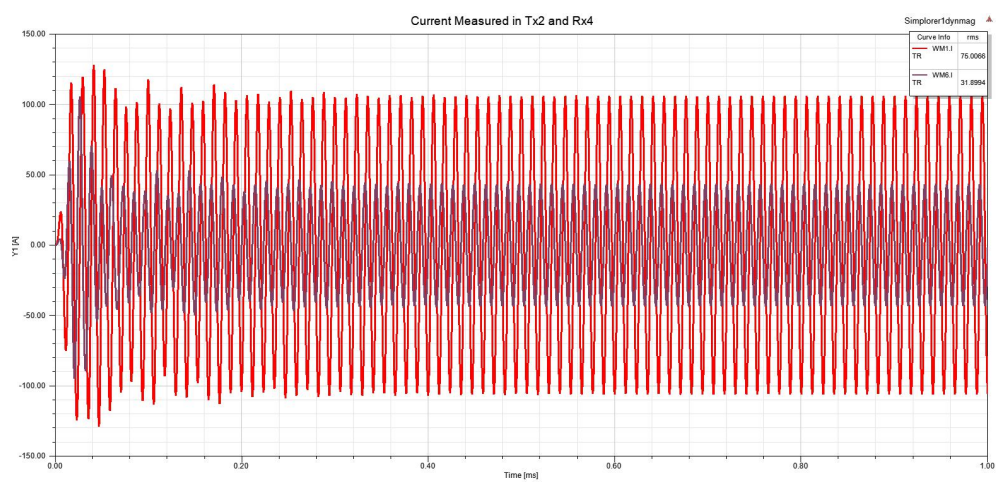After going through all the results and discussion we can conclude that the objective of this thesis to design a coil for higher power transfer has been verified and feasible as per the simulations performed in Ansys. But we have taken a ideal source and load so it is possible that with all the components in the circuit, the results may vary to an extent in the simulation part which is inevitable, still the design for the coil is correct and serves its purpose, even the misalignment tolerance can be found that it is better when used in this configuration of Bipolar pad in both transmitter and receiver side.

The implementation of LCC double sided compensation had its advantages of better misalignment tolerance, reactive power compensated to let the system work near to unity power factor. Further investigation with double sided LCC compensation can be carried out as an extension of this thesis which can be a further simulated analysis in Ansys simplorer by taking the converters and inverters involved in the system which has been neglected here, hence the results can be more accurate to actual world scenario. Even further simulation can be carried on interoperability with other wireless power transfer pad like cirular pad or DD pad and can be validated with interoperability efficiency and power transfers.

Hereby this thesis can be made as a starting point for further future analysis and hopefully can overcome the limitation present in the present day world of wireless power transfer.

Bibliography

[1] S. Chopra and P. Bauer. Analysis and design considerations for a contactless power transfer system. *INTELEC, International Telecommunications Energy Conference (Proceedings)*, pages 1–6, 2011.

[2] William C Brown. The History of Power Transmission by Radio Waves. *IEEE Transactions on Microwave Theory And Techniques*, M(9):1230–1242, 1984.

[3] J. O'Neill. *Prodigal Genius: The Life of Nicola Tesla*. Book Tree, 2007 edition.

[4] Zicheng Bi, Tianze Kan, Chunting Chris Mi, Yiming Zhang, Zhengming Zhao, and Gregory A. Keoleian. A review of wireless power transfer for electric vehicles: Prospects to enhance sustainable mobility. *Applied Energy*, 179:413–425, 2016.

[5] S. Y.R. Hui, Wenxing Zhong, and C. K. Lee. A critical review of recent progress in mid-range wireless power transfer. *IEEE Transactions on Power Electronics*, 29(9):4500–4511, 2014.

[6] Xiao Lu, Ping Wang, Dusit Niyato, Dong In Kim, and Zhu Han. Wireless Charging Technologies: Fundamentals, Standards, and Network Applications. *IEEE Communications Surveys and Tutorials*, 18(2):1413–1452, 2016.

[7] Chunhua Liu, Chaoqiang Jiang, and Chun Qiu. Overview of coil designs for wireless charging of electric vehicle. *2017 IEEE PELS Workshop on Emerging Technologies: Wireless Power Transfer, WoW 2017*, pages 1–6, 2017.

[8] Devendra Patil, Matthew K. McDonough, John M. Miller, Babak Fahimi, and Poras T. Balsara. Wireless Power Transfer for Vehicular Applications: Overview and Challenges. *IEEE Transactions on Transportation Electrification*, 4(1):3–37, 2017.

[9] J T Boys and G a Covic. IPT Fact Sheet Series: No.2 Magnetic Circuits for Powering Electric Vehicles. *Qualcomm*, (2), 2014.

[10] Mickel Budhia, Grant Covic, and John Boys. A new IPT magnetic coupler for electric vehicle charging systems. *IECON Proceedings (Industrial Electronics Conference)*, pages 2487–2492, 2010.

[11] Seho Kim, Grant A. Covic, and John T. Boys. Tripolar pad for inductive power transfer systems for EV charging. *IEEE Transactions on Power Electronics*, 32(7):5045–5057, 2017.

[12] Adeel Zaheer, Hao Hao, Grant A. Covic, and Dariusz Kacprzak. Investigation of multiple decoupled coil primary pad topologies in lumped IPT systems for interoperable electric vehicle charging. *IEEE Transactions on Power Electronics*, 30(4):1937–1955, 2015.

[13] Wei Zhang and Chunting Chris Mi. Compensation topologies of high-power wireless power transfer systems. *IEEE Transactions on Vehicular Technology*, 65(6):4768–4778, 2016.

[14] Robert W. Erickson and Dragan Maksimovic. *Fundametal of Power Electronic*. New York, NY, USA, 2001.

[15] Navid Rasekh and Mojtaba Mirsalim. Design of a compact and efficient Bipolar pad with a new integration of LCC compensation method for WPT. *9th Annual International Power Electronics, Drive Systems, and Technologies Conference, PEDSTC 2018*, 2018-Janua:44–47, 2018.

[16] Siqi Li, Weihan Li, Junjun Deng, Trong Duy Nguyen, and Chunting Chris Mi. A Double-Sided LCC Compensation Network and Its Tuning Method for Wireless Power Transfer. *IEEE Transactions on Vehicular Technology*, 64(6):2261–2273, 2015.

[17] M. Feliziani, T. Campi, S. Cruciani, F. Maradei, U. Grasselli, M. Macellari, and L. Schirone. Robust LCC compensation in wireless power transfer with variable coupling factor due to coil misalignment. *2015 IEEE 15th International Conference on Environment and Electrical Engineering, EEEIC 2015 - Conference Proceedings*, pages 1181–1186, 2015.

[18] Yang Yang, Mohamed El Baghdadi, Yuanfeng Lan, Yassine Benomar, Joeri Van Mierlo, and Omar Hegazy. Design methodology, modeling, and comparative study of wireless power transfer systems for electric vehicles. *Energies*, 11(7), 2018.

[19] Adeel Zaheer, Mickel Budhia, Dariusz Kacprzak, and Grant A. Covic. Magnetic design of a 300 W under-floor contactless Power Transfer system. *IECON Proceedings (Industrial Electronics Conference)*, pages 1408–1413, 2011.